Activation of Triiron Clusters by Electron Transfer. The Pronounced Modulation of ETC Catalysis by Bridging Ligands

T. M. Bockman and J. K. Kochi*

Contribution from the Department of Chemistry, University of Houston—University Park, Houston, Texas 77004. Received March 11, 1987

Abstract: The series of isostructural triiron clusters $Fe_3(CO)_9(\mu_3\text{-}E)_2$ (I) with the bridging ligands E = S, Se, NPh, and PPh undergo rapid and efficient electron-transfer chain (ETC) catalysis of ligand substitution. Electrostimulation at controlled negative potentials allows either mono- or disubstitution to be carried out selectively at 25 °C within 15 min of triiron clusters, which are otherwise inert to substitution. Unlike the thermal processes for I, which are insensitive to the nature of the bridging cap E, the rapid ETC catalysis of ligand substitution shows large differences of more than 10^6 in the comparative reactivity of the nitrogen and phosphorus analogues. Quantitative analysis of the kinetics for ETC catalysis derives from the digital simulation of the convoluted cyclic voltammograms of $Fe_3(CO)_9(\mu_3\text{-}S)_2$ obtained in the presence of the added ligand $P(OMe)_3$. Such studies demonstrate that ETC activation depends critically on the reactivity of the anion-radical intermediate $Fe_3(CO)_9(\mu_3\text{-}E)_2{}^{\bullet-}$ as it undergoes dissociative (first-order) loss of CO when E = S, Se, and NPh to generate the coordinatively unsaturated iron clusters. These clusters thus differ from the phosphorus analogue examined earlier in which the scission of the iron bond to the phosphinidene cap constituted the rate-limiting process to generate the 17-electron iron species in ETC catalysis. The experimental observation of the pronounced modulation of cluster reactivity in ETC catalysis by the bridging cap will hopefully encourage further theoretical analysis of the differences in bonding of open-shell systems. The monosubstituted cluster $Fe_3(CO)_8(\mu_3\text{-}NPh)_2[P(OMe)_3]$ crystallized in the triclinic space group, $P\bar{1}$, with the following cell constants: $a = 9.065$ (2), $b = 17.474$ (8), $c = 17.989$ (6) Å; $\alpha = 87.11$ (4), $\beta = 84.20$ (3), $\gamma = 88.35$ (4)°; $Z = 4$.

Active interest in transition-metal clusters derives from their conceptual relationship to catalytically active metal surfaces.[1] Indeed their delocalized structures, characteristic of metals, offer multisite access to various redox reactions as a result of contiguous metal centers.[2,3] Of particular interest among these are the series of rapid chain processes with metal carbonyls induced by oxidation–reduction,[4–9] for which the designation electron-transfer chain or ETC catalysis has been presented.[10,11] The importance of ETC catalysis lies in the facile activation of otherwise kinetically inert polynuclear clusters.[12] Even more important is the selectivity with which reactions can be carried out on cluster sites under the mild conditions extant in ETC catalysis.[6,13]

The oxidation–reduction properties of the trinuclear clusters of iron, ruthenium, and osmium carbonyls $M_3(CO)_{12}$ and various tricobalt alkylidyne carbonyls $XCCo_3(CO)_9$ have been recently examined in detail.[14–16] Their redox chemistry and the analysis of the ESR spectra, together with theoretical calculations of simple trinuclear clusters,[17] indicate that the LUMOS are primarily composed of metal–metal antibonding orbitals. This conclusion accounts for the tendency of metal carbonyl clusters to undergo fragmentation to species of lower nuclearity upon reduction.[18]

Cluster fragmentations have been successfully offset by the incorporation of strong bridging ligands, especially those centered around nitrogen, phosphorus, and the chalcogens.[2,19,20] It is generally assumed in these types of clusters that the bridging caps E serve mainly to hold the metal centers intact. For example, in the ligand substitution of a series of bicapped triiron carbonyl clusters $Fe_3(CO)_9(\mu_3\text{-}E)_2$ (I), the rates of the dissociative and associative pathways are not highly dependent on the nature of the caps with $\mu_3\text{-}E$ = S, Se, Te, NMe, and NPh.[21,22] However,

(1) (a) Muetterties, E. L.; Rhodin, T. N.; Band, E.; Brucker, C. F.; Pretzer, W. R. *Chem. Rev.* **1979**, *79*, 91. (b) Moskovitz, M. *Acc. Chem. Res.* **1979**, *12*, 229.

(2) (a) Johnson, B. F. G., Ed. *Transition Metal Clusters*; Wiley: New York, 1980. (b) Vahrenkamp, H. *Adv. Organomet. Chem.* **1983**, *22*, 167.

(3) (a) Ferguson, J. A.; Meyer, T. J. *J. Am. Chem. Soc.* **1972**, *94*, 3409. (b) Toan, T.; Teo, B. K.; Ferguson, J. A.; Meyer, T. J.; Dahl, L. E. *J. Am. Chem. Soc.* **1977**, *99*, 408. (c) Madach, T.; Vahrenkamp, H. *Chem. Ber.* **1981**, *114*, 505. (d) Lemoine, P. *Coord. Chem. Rev.* **1982**, *47*, 55. (e) Pickett, C. J. *J. Chem. Soc., Chem. Commun.* **1985**, 323.

(4) (a) Bezems, G. J.; Rieger, P. H.; Visco, S. *J. Chem. Soc., Chem. Commun.* **1981**, 265. (b) Bruce, M. I.; Kehoe, D. C.; Matisons, J. G.; Nicholson, B. K.; Riger, P. H.; Williams, M. L. *J. Chem. Soc., Chem. Commun.* **1982**, 442.

(5) (a) Darchen, A.; Mahe, C.; Patin, J. *J. Chem. Soc., Chem. Commun.* **1982**, 243. (b) Darchen, A.; Mahe, C.; Patin, H. *Nouv. J. Chim.* **1982**, *68*, 539. (c) See also: Lhadi, E. K.; Mahe, C.; Patin, H.; Darchen, A. *J. Organomet. Chem.* **1983**, *246*, C61.

(6) Darchen, A.; Mahe, C.; Patin, H. *Nouv. J. Chim.* **1983**, *7*, 453.

(7) Arewgoda, M.; Robinson, B. H.; Simpson, J. *J. Am. Chem. Soc.* **1983**, *105*, 1893.

(8) (a) Hershberger, J. W.; Kochi, J. K. *J. Chem. Soc., Chem. Commun.* **1982**, 212. (b) Richmond, M. G.; Kochi, J. K. *Inorg. Chem.* **1986**, *25*, 656, and references therein.

(9) (a) Peake, B. M.; Robinson, B. H.; Simpson, J.; Watson, D. J. *Inorg. Chem.* **1977**, *16*, 405. (b) Bond, A. M.; Dawson, P.; Peake, B. M.; Robinson, B. H.; Simpson, J. *Inorg. Chem.* **1979**, *18*, 1413.

(10) Kochi, J. K. *J. Organomet. Chem.* **1986**, *300*, 139.

(11) For general discussion of ETC mechanisms, see: (a) Chanon, M.; Tobe, M. L. *Angew. Chem., Int. Ed. Engl.* **1982**, *21*, 1. (b) Bunnett, J. F. *Acc. Chem. Res.* **1978**, *11*, 413. (c) Saveant, J. M. *Acc. Chem. Res.* **1980**, *13*, 323. (d) Chanon, M. *Bull. Soc. Chim. Fr.* **1982**, 197.

(12) See, e.g.: Treichel, P. M.; Dean, W. K.; Douglas, W. M. *Inorg. Chem.* **1972**, *11*, 1609.

(13) Ohst, H. H.; Kochi, J. K. *J. Am. Chem. Soc.* **1986**, *108*, 2897.

(14) Bond, A. M.; Dawson, P. A.; Peake, B. M.; Robinson, B. H.; Simpson, J. *Inorg. Chem.* **1977**, *16*, 2199. See also: Cyr, J. C.; DeGray, J. A.; Gosser, D. K.; Lee, E. S.; Rieger, P. H. *Organometallics* **1985**, *4*, 950.

(15) X represents either a heteroatom or a carbon-centered group. (a) Dessey, R. E.; King, R. B.; Waldrop, M. *J. Am. Chem. Soc.* **1966**, *88*, 5112. (b) Kotz, J. C.; Petersen, J. V.; Reed, R. C. *J. Organomet. Chem.* **1976**, *120*, 433. (c) Peake, B. M.; Reiger, P. H.; Robinson, B. H.; Simpson, J. *Inorg. Chem.* **1981**, *20*, 2540. (d) Bond, A. M.; Dawson, P. A.; Peake, B. M.; Rieger, P. H.; Robinson, B. H.; Simpson, J. *Inorg. Chem.* **1979**, *18*, 1413. (e) Peake, B. M.; Robinson, B. H.; Simpson, J.; Watson, D. J. *Inorg. Chem.* **1977**, *16*, 405. (f) Bond, A. M.; Peake, B. M.; Robinson, B. H.; Simpson, J.; Watson, D. J. *Inorg. Chem.* **1977**, *16*, 410.

(16) (a) Colbran, S. B.; Robinson, B. H.; Simpson, J. *Organometallics* **1983**, *2*, 943. (b) Colbran, S. B.; Robinson, B. H.; Simpson, J. *Organometallics* **1983**, *2*, 952. (c) Colbran, S. B.; Robinson, B. H.; Simpson, J. *J. Organomet. Chem.* **1984**, *265*, 199. (d) Lindsay, P. N.; Peake, B. M.; Robinson, B. H.; Simpson, J.; Honrath, U.; Vahrenkamp, H.; Bond, A. M. *Organometallics* **1984**, *3*, 413. (e) Benoit, A.; Darchen, A.; LeMaroville, J.; Mahe, C.; Patin, H. *Organometallics* **1983**, *2*, 555. (f) See also ref 3a.

(17) Schillling, B. E. R.; Hoffman, R. *J. Am. Chem. Soc.* **1979**, *101*, 3456.

(18) (a) Vahrenkamp, H. *Struct. Bonding (Berlin)* **1977**, *32*, 1. (b) Deeming, A. J. *Transition Metal Clusters*; Johnson, B. F. G., Ed.; Wiley: New York, 1980; Chapter 6. (c) Pittman, C. U., Jr.; Richmond, M. G.; Absi-Halibi, M.; Vahrenkamp, H.; Richter, F.; Beurich, H. *Angew. Chem., Int. Ed. Engl.* **1982**, *21*, 786. (d) Richmond, M. G.; Pittman, C. U., Jr.; Absi-Halibi, M. *J. Mol. Catal.* **1984**, *22*, 367.

(19) See also: (a) Ryan, R. C.; Dahl, L. F. *J. Am. Chem. Soc.* **1975**, *97*, 6904. (b) Ryan, R. C.; Pittman, C. U., Jr.; O'Connor, J. P.; Dahl, L. F. *J. Organomet. Chem.* **1980**, *193*, 247. (c) Kouba, J. K.; Muetterties, E. L.; Thompson, M. R.; Day, V. W. *Organometallics* **1983**, *2*, 1065.
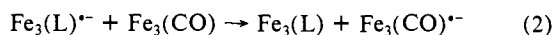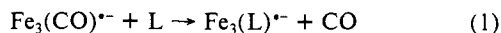
(20) For the effect of capping bridges on cluster stability, see: (a) Vahrenkamp, H.; Keller, E. *Chem. Ber.* **1979**, *109*, 229. (b) Langenbach, H. J.; Vahrenkamp, H. *Chem. Ber.* **1979**, *112*, 3390. (c) Langenbach, H. J.; Keller, E.; Vahrenkamp, J. *J. Organomet. Chem.* **1979**, *171*, 259.
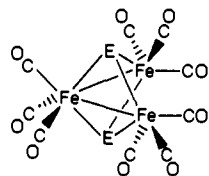
1: E = NPh or NAn, S, Se. PPh

in a recent study of the phosphorus-capped analogue $Fe_3(CO)_9$-$(\mu_3$-PPh$)_2$, we found that the ETC catalysis of ligand substitution depended on the intimate involvement of the phosphinidene bridging ligand.[13] Since the role of the bridging cap on cluster reactivity during ETC catalysis has not been quantitatively assessed, we examined the triiron carbonyls with other bridging caps such as nitrogen, sulfur, and selenium. Coupled with the earlier report of the related cluster $Fe_3(CO)_8G(\mu_3$-S$)_2$ where G was a dithiocarbene,[6] we are particularly concerned with the *rate* of the critical substitution step (Scheme I, eq 1) in the generalized

Scheme I

$$Fe_3(CO)^{\cdot-} + L \rightarrow Fe_3(L)^{\cdot-} + CO \qquad (1)$$

$$Fe_3(L)^{\cdot-} + Fe_3(CO) \rightarrow Fe_3(L) + Fe_3(CO)^{\cdot-} \qquad (2)$$

formulation for the propagation sequence in ETC catalysis, as depicted above, where Fe_3 represents the triiron moiety Fe_3-$(CO)_8(\mu_3$-E$)_2$ and L is a nucleophile. Initiation of ETC catalysis can be effected by either chemical or electrochemical reduction of the triiron cluster,[23] i.e. eq 3. In this study we have exploited

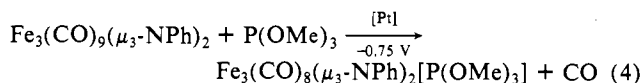$$Fe_3(CO) \xrightarrow{+e^-} Fe_3(CO)^{\cdot-} \qquad (3)$$
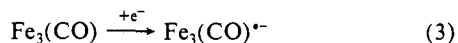
the versatility of the electrochemical techniques to probe the effect of the bridging caps on the ETC catalysis of ligand substitution in the series of isostructural triiron clusters I. Trimethyl phosphite was selected as the common nucleophilic ligand L.

Results

Synthesis of Bicapped Triiron Carbonyl Clusters I with μ_3-E = S, Se, and NPh. The family of the structurally related triiron clusters $Fe_3(CO)_9(\mu_3$-E$)_2$ (I) was available from distinctly different synthetic procedures. Thus, the phenylphosphinidene analogue with E = PPh was prepared originally by Treichel and co-workers from the thermolysis of iron pentacarbonyl and phenylphosphine at 190 °C.[12] On the other hand, the sulfur and selenium derivatives with E = S and Se, respectively, can be isolated in low yields ($\sim$20%) from the redox reaction of iron pentacarbonyl with sulfite and selenite by the method of Hieber and Gruber.[24] Finally the phenylnitrene analogue with E = NPh and N(C$_6$H$_4$-p-OMe) was synthesized from the reaction of iron dodecacarbonyl with nitrobenzene and p-nitroanisole, respectively.[25] The low yields (<10%) of the triiron clusters were accompanied by a complex mixture of highly colored byproducts.
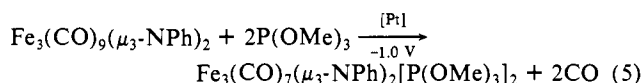
ETC Catalysis of Ligand Substitution. Products and Stoichoimetry. The triiron clusters $Fe_3(CO)_9(\mu_3$-E$)_2$ with E = S, Se, and NAryl are all relatively stable to ligand substitution by trimethyl phosphite in tetrahydrofuran at 25 °C (see the Experimental Section). However, phosphite substitution was effected rapidly if a set of platinum electrode [Pt] was simply inserted into the THF solution and a slight negative potential applied.[26] For example, the results in Table I show that ligand substitution was completed within 15 min at 25 °C when the nitrogen analogue

with E = NPh was treated with 2 equiv of trimethyl phosphite at -0.75 V vs. SCE. Isolation of the dark red-purple crystals in 70% yield followed by elemental analysis indicated that only the monosubstitution of a single carbonyl ligand took place with the stoichiometry in eq 4.

$$Fe_3(CO)_9(\mu_3\text{-NPh})_2 + P(OMe)_3 \xrightarrow[-0.75 \text{ V}]{[Pt]}$$
$$Fe_3(CO)_8(\mu_3\text{-NPh})_2[P(OMe)_3] + CO \quad (4)$$

The course of ligand substitution under electrostimulation was followed during bulk electrolysis at constant potential by periodically extracting an aliquot of the catholyte and measuring the disappearance of the high-frequency carbonyl band at 2085 cm^{-1} in the infrared spectrum. More conveniently, the cathodic current in the potentiostatic experiment was observed to be relatively invariant at $\sim$5 mA for approximately 15 min, whereupon it abruptly diminished to zero. The latter signaled the completion of the ligand substitution, as confirmed by IR analysis of the catholyte. The electrocatalytic nature of the substitution was readily deduced from the measurement of the amount of current (faradays) passed through the solution. A turnover number (TN)[27] in excess of 600 equiv of monosubstitution product per electron was obtained for eq 4. Similarly the anisylnitrene analogue (E = NC$_6$H$_5$-p-OMe) yielded the monophosphite derivative cleanly with TN = 45 when the potential was controlled at -0.75 V. Only the monosubstituted derivatives of the sulfur and selenium analogues (E = S and Se) were isolated as dark red crystals in 48 and 54% yields, respectively, with TN $\simeq$ 20 when a constant potential of -0.55 V was applied to solutions of the triiron clusters containing 2–4 equiv of trimethyl phosphite.

Multiple substitution of the triiron clusters I could be carried out in three ways. Thus, if the more negative potential of -1.0 V was applied to the nitrogen analogue under otherwise the same conditions as those in eq 4, the disubstituted derivative was isolated in 68% yield in a single step with TN = 60. Isolation of the purple crystals followed by elemental analysis confirmed that disubstitution of a pair of carbonyl ligands took place with the stoichiometry in eq 5. No contamination by the monosubstitution

$$Fe_3(CO)_9(\mu_3\text{-NPh})_2 + 2P(OMe)_3 \xrightarrow[-1.0 \text{ V}]{[Pt]}$$
$$Fe_3(CO)_7(\mu_3\text{-NPh})_2[P(OMe)_3]_2 + 2CO \quad (5)$$

product was observed. Essentially the same yield of pure disubstitution product was obtained with TN = 59, if the monosubstitution product $Fe_3(CO)_8(\mu_3$-NPh$)_2[P(OMe)_3]$ was first isolated and then resubjected to trimethyl phosphite at -1.0 V. Alternatively, the parent triiron cluster could be treated with excess trimethyl phosphite and the applied potential stepped sequentially from -0.55 to -0.90 V, as with the selenium analogue (see Table I). Only the monosubstituted derivative was observed in the first stage ($\sim$10 min) with TN = 100, and only the disubstituted product was isolated in 63% with TN = 53 in the second stage (10 min). The latter offers a striking example of the high selectivity that is possible in ETC catalysis by the simple adjustment of the applied potential. In contrast, the thermal process for the ligand substitution of these triiron clusters with triphenyl phosphite or various phosphines and arsines has been reported to give mixtures consisting mainly of mono- and disubstitution products.[21,22]

Structure and Stereochemistry in Ligand Substitution of Triiron Carbonyl Clusters. The triiron carbonyl clusters all share in common IR spectra with a weak band at $\sim$2100 cm^{-1}, which increases more or less with the electronegativity of the capping atom (Table II). This band is tentatively assigned to the totally symmetric carbonyl stretching mode (A$_1$) of the carbonyl cluster, since its intensity increases markedly upon monosubstitution (of phosphite).

The phosphite ligand in the monosubstituted nitrene analogue $Fe_3(CO)_8(\mu_3$-NPh$)_2[P(OMe)_3]$ showed a sharp singlet resonance

(21) See: (a) Cetini, G.; Stanghellini, P. L.; Rossetti, R.; Gambino, O. *J. Organomet. Chem.* **1968**, *15*, 373. (b) Cetini, G.; Stanghellini, P. L.; Rossetti, R.; Gambino, O. *Inorg. Chim. Acta* **1968**, *2*, 433. (c) Rossetti, R.; Stanghellini, P. L.; Gambino, O.; Cetini, G. *Inorg. Chim. Acta* **1972**, *6*, 205.

(22) (a) Rossetti, R.; Stanghellini, P. L. *J. Coord. Chem.* **1974**, *3*, 217. (b) Rossetti, R.; Gervasio, G.; Stanghellini, P. L. *J. Chem. Soc., Dalton Trans.* **1978**, 222. (c) Lesch, D. A.; Rauchfuss, T. B. *Organometallics* **1982**, *1*, 499, and ref 10–15 cited therein.

(23) Ohst, H. H.; Kochi, J. K. *Inorg. Chem.* **1986**, *25*, 2066.

(24) Hieber, W.; Gruber, J. *Z. Anorg. Allg. Chem.* **1958**, *296*, 91.

(25) Landesberg, J. M.; Katz, L.; Olsen, C. *J. Org. Chem.* **1972**, *37*, 930.

(26) These studies were all carried out in the presence of 0.2 M tetra-*n*-butylammonium perchlorate (TBAP) as the supporting electrolyte.

(27) The catalytic turnover number is defined as the moles of product formed per faraday of charge required.

Table I. ETC Catalysis of Ligand Substitution of $Fe_3(CO)_9(\mu_3\text{-}E)_2$ with E = S, Se, and NPh^a

triiron cluster	added cluster, mmol	added $L,^b$ mmol	solvent	potential,^{c} V (%)	product	yield,^{d} %	TN^e
$Fe_3(CO)_9(\mu_3\text{-}S)_2$	0.39	1.68	THF	−0.55 (5)	$Fe_3(CO)_8S_2L$	48	18
$Fe_3(CO)_8(\mu_3\text{-}S)_2[P(OMe)_3]$	0.28	1.18	THF	−0.80 (16)	$Fe_3(CO)_7S_2L_2$	45	6.3
$Fe_3(CO)_9(\mu_3\text{-}Se)_2$	0.26	0.52	CH_2Cl_2	−0.55 (2.7)	$Fe_3(CO)_8Se_2L$	54	37
$Fe_3(CO)_9(\mu_3\text{-}Se)_2$	0.46	2.28	THF	−0.60 (1.0) −0.90 (1.9)	$Fe_3(CO)_7Se_2L_2$	63	53
$Fe_3(CO)_9(\mu_3\text{-}NPh)_2$	0.38	0.85	THF	−0.75 (0.16)	$Fe_3(CO)_8(NPh)_2L$	69	614
$Fe_3(CO)_9(\mu_3\text{-}NAn)_2$	0.25	0.43	THF	−0.71 (2.2)	$Fe_3(CO)_8(NAn)_2L$	45	45
$Fe_3(CO)_9(\mu_3\text{-}NPh)_2$	0.19	0.42	THF	−1.0 (1.7)	$Fe_3(CO)_7(NPh)_2L_2$	68	59

^{a} In 20 mL of solvent containing 0.2 M TBAP at room temperature. ^{b} Trimethyl phosphite. ^{c} Potentiostatic mode, V vs SCE. Coulometric charge represented as percent based on $Fe_3(CO)_9(E)_2$ in parentheses. ^{d} Isolated as crystalline cluster. ^{e} Turnover number.

Table II. Infrared Spectra (ν_{CO}) of the Triiron Clusters^{a,b}

$Fe_3(CO)_9(\mu_3\text{-}NC_6H_5)_2$	2085 (w), 2056, 2033, 2014, 2009
$Fe_3(CO)_8(\mu_3\text{-}NC_6H_5)_2[P(OCH_3)_3]$	2066 (m), 2025, 2010, 2003, 1969, 1964
$Fe_3(CO)_7(\mu_3\text{-}NC_6H_5)_2[P(OCH_3)_3]_2$	2050 (m), 2025, 2006, 1988, 1979, 1964, 1954
$Fe_3(CO)_9(\mu_3\text{-}Se)_2$	2090 (vw), 2056, 2038, 2017, 2013, 1983 (w)
$Fe_3(CO)_8(\mu_3\text{-}Se)_2[P(OCH_3)_3]$	2070 (m), 2045, 2031, 2006, 1976 (m)
$Fe_3(CO)_7(\mu_3\text{-}Se)_2[P(OCH_3)_3]_2$	2051 (m), 2010, 1990, 1979, 1968, 1959 (m)
$Fe_3(CO)_9(\mu_3\text{-}S)_2$	2093 (vw), 2062, 2045, 2023, 2007 (m)
$Fe_3(CO)_8(\mu_3\text{-}S)_2[P(OCH_3)_3]$	2076 (m), 2050, 2037, 2012, 2000, 1992 (m), 1986 (m)
$Fe_3(CO)_7(\mu_3\text{-}S)_2[P(OCH_3)_3]_2$	2056 (m), 2016, 1995, 1985, 1974, 1936 (w)

^{a} n-Hexane solution. ^{b} All bands strong unless specified otherwise.

Table III. ^1H and ^{31}P NMR of the Triiron Clusters^a

triiron cluster	^{31}P NMR, ppm	^1H NMR, ppm
$Fe_3(CO)_8(\mu_3\text{-}S)_2[P(OCH_3)_3]$	165.1 (s), 168.8 (s)	3.85 (d, $^2J(^1H^{31}P)$ = 12 Hz), 3.79 (d, $^2J(^1H^{31}P)$ = 12 Hz)
$Fe_3(CO)_7(\mu_3\text{-}S)_2[P(OCH_3)_3]_2$	176.1 (d, $J(^{31}P^{31}P)$ = 8 Hz), 171.6 (d, $J(^{31}P^{31}P)$ = 8 Hz), 169.3 (br s)	b
$Fe_3(CO)_8(\mu_3\text{-}Se)_2[P(OCH_3)_3]$	168.7 (s), 171.3 (s)	3.82 (d, $^2J(^1H^{31}P)$ = 12 Hz), 3.74 (d, $^2J(^1H^{31}P)$ = 12 Hz)
$Fe_3(CO)_7(\mu_3\text{-}Se)_2[P(OCH_3)_3]_2$	178.7 (d, $J(^{31}P^{31}P)$ = 8 Hz), 174.3 (d, $J(^{31}P^{31}P)$ = 8 Hz), 171.8 (br s)	b
$Fe_3(CO)_8(\mu_3\text{-}NC_6H_5)_2[P(OCH_3)_3]$	158.5 (s)	3.52 (d, $J(^1H^{31}P)$ = 11 Hz, (9 H)), 7.11 (br s (10 H))
$Fe_3(CO)_7(\mu_3\text{-}NC_6H_5)_2[P(OCH_3)_3]_2$	167.2 (d, $J(^{31}P^{31}P)$ = 13 Hz), 159.7 (d, $J(^{31}P^{31}P)$ = 13 Hz)	3.65 (d, $J(^1H^{31}P)$ = 10.8 Hz (9 H)), 3.45 (d, $J(^1H^{31}P)$ = 10.7 Hz (9 H)), 6.97 (br s (5 H))

^{a} In $CDCl_3$ solution at room temperature. ^{b} Multiplet, δ 3.9–3.2.

at δ 158.5 in the $^{31}P\{^1H\}$ NMR spectrum and a doublet at δ 3.52 (J_{H-P} = 11 Hz) in the ^1H NMR spectrum (Table III). The temperature-independent line widths of both resonances accorded with a relatively static axial conformation of $P(OMe)_3$ located on one of the basal iron atoms, as defined by Muetterties et al. for the phenylphosphinidene analogue.[19c] This conclusion was borne out following the successful isolation and growth of a single crystal for the X-ray diffraction analysis. The ORTEP diagram in Figure 1 shows $Fe_3(CO)_8(\mu_3\text{-}NPh)_2[P(OMe)_3]$ to be structurally related to the parent cluster by substitution of phosphite at the basal Fe1.[28] Stereochemically, the phosphite ligand occupies an axial conformation, which persists in solution. [For a detailed structural analysis of $Fe_3(CO)_8(\mu_3\text{-}NPh)_2[P(OMe)_3]$, see the Experimental Section.] The temperature-invariant ^{31}P NMR spectrum of $Fe_3(CO)_8(\mu_3\text{-}NPh)_2[P(OMe)_3]$ accords with the absence of equatorial–axial site exchange, which is characteristic of monosubstituted bicapped triiron clusters.[29]

We judge from the similarity of the IR bands in the carbonyl stretching region (see Table II) that the anisyl analogue $Fe_3(CO)_8(\mu_3\text{-}NC_6H_4\text{-}p\text{-}OMe)_2[P(OMe)_3]$ has basically the same structure as that shown in Figure 1 for the phenylnitrene complex.

The monosubstitution product derived from the sulfur analogue consisted of a mixture of monosubstitution products, as judged by the presence of a pair of singlets at δ 165.1 and 168.8 with an intensity ratio of 1:4 in the $^{31}P\{^1H\}$ NMR spectrum. The same relative intensities pertained to the doublet ^1H resonances at δ

(28) Compare with the N-methyl analogue: Doedens, R. J. *Inorg. Chem.* **1969**, *8*, 570.

(29) See, e.g.: Muetterties et al. in ref 19c and Ohst in ref 13.

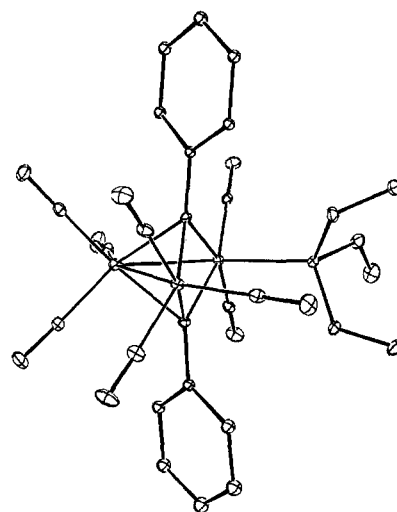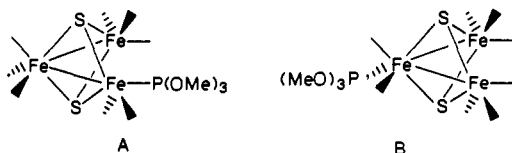**Figure 1.** ORTEP diagram of the monosubstitution product from the ETC catalysis of $Fe_3(CO)_9(\mu_3\text{-}NPh)_2$ with trimethyl phosphite. Hydrogen atoms are omitted for clarity.

3.85 and 3.79 (J_{H-P} = 12.3 Hz) for the methoxy groups in $Fe_3(CO)_8(\mu_3\text{-}S)_2[P(OMe)_3]$. The major isomer A was assigned to ligand substitution at the basal Fe1, owing to a temperature-dependent broadening of the ^{31}P resonance at δ 168.8 (compare Figure 9 in the Experimental Section). By contrast, the minor isomer B with the ^{31}P resonance at δ 165.1 showed no line broadening, and it was assigned to the product of apical substi-

7728 *J. Am. Chem. Soc., Vol. 109, No. 25, 1987*

Bockman and Kochi

A. Argon

B. Carbon Monoxide

Figure 2. Reversible cyclic voltammogram of 5×10^{-3} M Fe$_3$(CO)$_9$-(μ_3-NPh)$_2$ in dichloromethane containing 0.1 M TBAP under (A) an argon and (B) a carbon monoxide atmosphere at a scan rate of 200 mV s^{-1}. For the significance of the CV peak N, see text.

tution. Such a conclusion derives from the previous rigorous analysis of the temperature-dependent ^{13}C NMR spectra for the P(OPh)$_3$ derivative of the sulfur analogue.[30,31] This assignment also accords with the relative phosphite chemical shifts in the ^{31}P NMR spectra of the corresponding isomers derived from the phosphorus analogue.[13] The composition of the mixture of monophosphites was unchanged when the solution was allowed to stand for prolonged periods or even when it was heated at 65 °C for 24 h. It is interesting to note that the thermal substitution of Fe$_3$(CO)$_9$(μ_3-S)$_2$ with trimethyl phosphite in THF solution at 65 °C afforded a fraction consisting of monosubstitution products with the same 4:1 ratio of A and B isomers.[32] Moreover, the selenium analogue upon treatment with trimethyl phosphite under ETC conditions produced an isomeric mixture of monosubstitution products with the same composition (see Table III).

The disubstitution product Fe$_3$(CO)$_7$(μ_3-NPh)$_2$[P(OMe)$_3$]$_2$ obtained from the nitrogen analogue had a relatively straightforward pattern of carbonyl stretching bands in the IR spectrum (Table II). This coupled with the observation of a 1:1 doublet at δ 159.7 and 167.2 (J_{P-P} = 13 Hz) in the proton-decoupled ^{31}P NMR spectrum together with a pair of equal doublets at δ 3.45 and 3.65 (J_{H-P} = 10.7 Hz) in the ^{1}H NMR spectrum was consistent with the presence of a single isomer. Moreover, the isolated yield of pure crystalline product in ~70% yield indicated that no other isomer was formed in significant amounts. Of the possible structures for Fe$_3$(CO)$_7$(μ_3-NPh)$_2$[P(OMe)$_3$]$_2$, we consider apical/basal isomer C to be more likely than the basal/basal isomer D, owing to the interligand coupling of the vicinal phosphites in
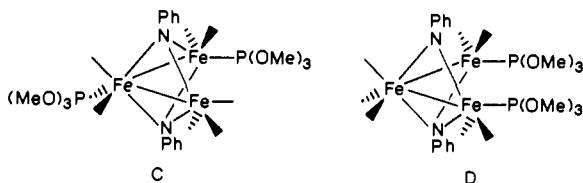
the ^{31}P{^{1}H} NMR spectrum described above.[33] The disubstitution products from the sulfur and selenium analogues appeared to consist of a mixture of isomers. For example, the proton-decoupled ^{31}P NMR spectrum of the selenium derivative Fe$_3$(CO)$_7$(μ_3-Se)$_2$[P(OMe)$_3$]$_2$ consisted of a pair of 1:1 doublets at δ 174.3 and 178.7 (J_{P-P} = 8 Hz) together with a broad singlet at δ 171.8 in a integration ratio of ~1:1:1 (Table III). We tentatively assign the pair of doublets to the major isomer (69%) with the apical/basal phosphites similar to C and the broad singlet[34] to the minor isomer (31%) with basal/basal phosphites similar to D. The disubstitution product from the sulfur analogue showed similarly complex IR, ^{31}P NMR, and ^{1}H NMR spectra, and it was not examined further.

Redox Properties of the Triiron Clusters Fe$_3$(CO)$_9$(μ_3-E)$_2$ with E = S, Se, and NPh. The preparative synthesis of the phosphite derivatives from each triiron cluster in Table I is controlled by

Table IV. Electrochemical Parameters for the Initial Reduction of Various Triiron Clusters[a]

triiron cluster	$-E_p{}^c$	$-E_p{}^a$	$-E^{0\,b}$
Fe$_3$(CO)$_9$(μ_3-S)$_2$	0.68	0.55	0.61
Fe$_3$(CO)$_9$(μ_3-Se)$_2$	0.61	0.51	0.56
Fe$_3$(CO)$_9$(μ_3-NC$_6$H$_5$)$_2$	0.98	0.76	0.86
Fe$_3$(CO)$_9$(μ_3-NC$_6$H$_5$)$_2{}^c$	0.77	0.66	0.71
Fe$_3$(CO)$_8$(μ_3-NC$_6$H$_5$)$_2$[P(OCH$_3$)$_3$]	1.13	0.80	0.96
Fe$_3$(CO)$_7$(μ_3-NC$_6$H$_5$)$_2$[P(OCH$_3$)$_3$]$_2$	1.43		d
Fe$_3$(CO)$_9$(μ_3-PPh)$_2$			0.79^e
Fe$_3$(CO)$_8$(μ_3-PPh)$_2$[P(OMe)$_3$]			1.09^e

^{a} In dichloromethane containing 0.1 M TBAP at 500 mV s^{-1}, unless indicated otherwise. ^{b} Taken as the average of the cathodic and anodic peak potentials in columns 3 and 4.[37] ^{c} In THF with 0.1 M TBAP. ^{d} Irreversible at this scan rate. ^{e} From ref 13.

the applied negative potential. The value of E_p determines the selectivity in ligand substitution by selecting the particular triiron carbonyl cluster to be reduced to its labile anion radical.[35] As such, we examined the cathodic behavior of each triiron cluster, both in the absence and in the presence of added trimethyl phosphite.

The electrochemical reduction of triiron carbonyls is best considered from the typical cyclic voltammogram (CV) in Figure 2, which shows the reversible wave for a one-electron reduction in eq 6,

$$\text{Fe}_3(\text{CO})_9(\mu_3\text{-E})_2 + e^- \rightleftharpoons \text{Fe}_3(\text{CO})_9(\mu_3\text{-E})_2{}^{\bullet-} \qquad (6)$$
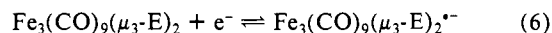
as judged by comparison with ferrocene as a calibrant.[36] The cathodic peak potential $E_p{}^c$ = -0.77 V vs SCE coupled with the associated anodic peak potential $E_p{}^a$ = -0.66 V yields a reduction potential of -0.71 V (Table IV) for the nitrene cluster Fe$_3$-(CO)$_9$(μ_3-NPh)$_2$.[37] Furthermore, the initial cathodic wave with $E_p{}^c$ = -0.77 V obtained under an argon atmosphere in Figure 2A is unchanged relative to that obtained under a CO atmosphere in Figure 2B. However, the presence of an additional cathodic wave N in Figure 2A, which is notably absent in Figure 2B, strongly suggests that the anion radical is metastable and subject to rapid, dissociative decomposition.[38] The latter is also indicated by the ratio of anodic and cathodic peak currents of unity under a CO atmosphere but of only 0.8 under argon (i.e., $i_p{}^a/i_p{}^c$ = 1.0 and 0.8 in parts B and A of Figure 2, respectively). Finally, at sufficiently high CV scan rates ($v > 800$ V s^{-1}), the additional cathodic wave N in Figure 2A was absent, owing to the oxidation

(30) Aime, S.; Milone, L.; Rossetti, R.; Stanghellini, P. L. *J. Chem. Soc., Dalton Trans.* **1979**, 46.

(31) The difference in the ^{31}P line-broadening behavior of the nitrogen and sulfur analogues may be attributed to the increased separation between the nonbonded Fe1 and Fe3; see Table V.

(32) Wang, Y., unpublished results.

(33) (a) For the apical-basal interligand coupling in the diphos derivative of the phosphorus analogue, see ref 13. (b) Of the two apical-basal isomers, we tentatively favor the axial conformer since the equatorial phosphite ligands resonate 10-15 ppm upfield from the axial conformer in the example above.[13] **Note Added in Proof:** The structural assignment of the phenylnitrene cluster Fe$_3$(CO)$_7$(μ_3-NPh)$_2$[P(OMe)$_3$]$_2$ as the apical, basal isomer C has been confirmed by X-ray crystallography.

(34) Apical phosphites are unlikely to show line broadening, owing to rapid site exchange, as observed in the ^{13}C NMR spectra.[30]
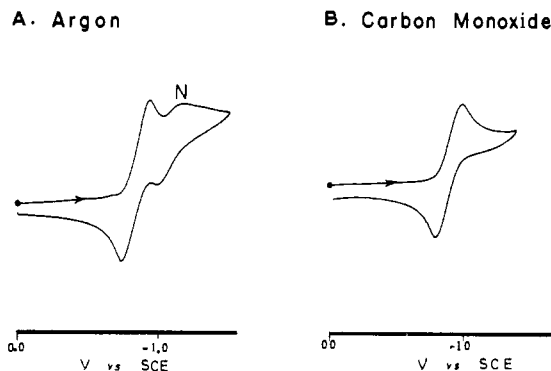
(35) Compare the similar behavior of the phosphinidenes and (carbene) sulfene clusters.[6,13]

(36) Gagne, R. R.; Koval, C. A.; Lisensky, G. C. *Inorg. Chem.* **1980**, *19*, 2854.

(37) See footnote 6 in: Howell, J. O.; Goncalves, J. M.; Amatore, C.; Klasinc, L.; Wightman, R. M.; Kochi, J. K. *J. Am. Chem. Soc.* **1984**, *106*, 3968.

(38) For a similar CV behavior in mononuclear carbonyls, see: Kuchynka, D. J; Amatore, C.; Kochi, J. K. *Inorg. Chem.* **1986**, *25*, 4087.
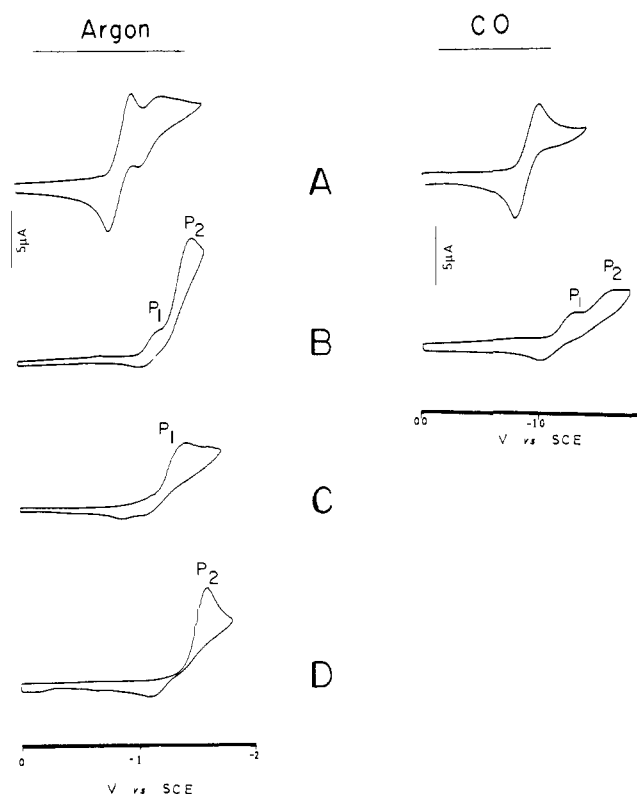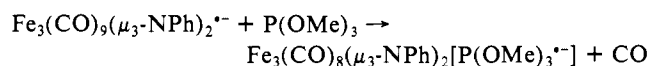
Figure 3. Cyclic voltammograms under an argon atmosphere (left) and under a CO atmosphere (right) of 5×10^{-3} M $Fe_3(CO)_9(\mu_3\text{-NPh})_2$ in dichloromethane containing 0.1 M TBAP at a scan rate of 200 mV s^{-1} with (A) no additive and (B) 15 equiv of added trimethyl phosphite. Cyclic voltammograms of authentic samples of the mono- and disubstitution products $Fe_3(CO)_8(\mu_3\text{-NPh})_2[P(OMe)_3]$ and $Fe_3(CO)_7(\mu_3\text{-NPh})_2[P(OMe)_3]_2$ under comparable conditions are shown by CV waves P_1 and P_2 in C and D, respectively.

of $Fe_3(CO)_9(\mu_3\text{-NPh})_2^{\cdot-}$ on the return sweep, which was faster than ligand dissociation in eq 7.

$$Fe_3(CO)_9(\mu_3\text{-NPh})_2^{\cdot-} \rightarrow CO + Fe_3(CO)_8(\mu_3\text{-NPh})_2^{\cdot-} \quad (7)$$
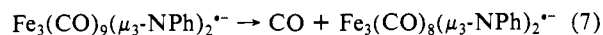
Although the anion radical was persistent on the CV time scale of $\sim 10^{-2}$ s, it was not sufficient to allow the ESR spectrum to be measured even at -20 °C under a CO atmosphere.[39]

The enhanced lability of the anion radical was also apparent in cyclic voltammograms of $Fe_3(CO)_9(\mu_3\text{-NPh})_2$ obtained in the presence of added trimethyl phosphite, as shown in Figure 3. The complete transformation of the cyclic voltammograms of $Fe_3(CO)_9(\mu_3\text{-NPh})_2$ in Figure 3A into those shown in Figure 3B was diagnostic of the extensive ligand substitution of $P(OMe)_3$ into the triiron cluster, since the new CV waves P_1 and P_2 coincided with those of the authentic mono- and disubstitution products $Fe_3(CO)_8(\mu_3\text{-NPh})_2[P(OMe)_3]$ and $Fe_3(CO)_7(\mu_3\text{-NPh})_2[P(OMe)_3]_2$ shown in parts C and D of Figure 3, respectively. It is also noteworthy that relatively more disubstitution product was formed under an argon atmosphere compared to that under a CO atmosphere, as shown by a comparison of the ratio of the peak currents for P_1 and P_2 in the left part and the right part of Figure 3B. It is important to emphasize that the cyclic voltammograms of $Fe_3(CO)_9(\mu_3\text{-NPh})_2$ in the presence of excess $(2 \times 10^{-2}$ M) $P(OMe)_3$ under an argon atmosphere consisted of only the reversible 1-electron redox couple at $E^0 = -0.71$ V at the fast scan rates of $v \geq 5000$ V s^{-1}. Thus these high scan rates are clearly sufficient to avoid the interception of $Fe_3(CO)_9(\mu_3\text{-NPh})_2^{\cdot-}$ by the added phosphite by a process such as

$$Fe_3(CO)_9(\mu_3\text{-NPh})_2^{\cdot-} + P(OMe)_3 \rightarrow$$
$$Fe_3(CO)_8(\mu_3\text{-NPh})_2[P(OMe)_3^{\cdot-}] + CO$$

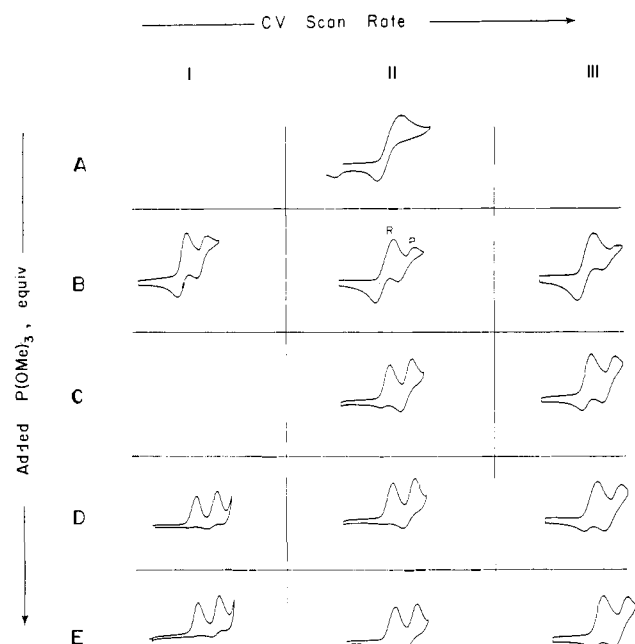(39) Further collaborative ESR studies are in progress with Dr. P. H. Rieger.

Figure 4. Cyclic voltammograms under an argon atmosphere of 6×10^{-3} M $Fe_3(CO)_9(\mu_3\text{-S})_2$ in dichloromethane containing 0.1 M TBAP and (A) 0, (B) 1.3, (C) 3.8, (D) 10.5, and (E) 20.8 equiv of added trimethyl phosphite at sweep rates of (I) 100, (II) 200, and (III) 500 mV s^{-1}.

In order to examine more closely the enhanced ligand substitution of the triiron clusters under cyclic voltammetric conditions we systematically varied the concentration of the added trimethyl phosphite. For these studies, we utilized the sulfur analogue since the extraneous competition from the slower disubstitution of this triiron cluster under CV conditions did not present a complicating factor. Cyclic voltammetry of $Fe_3(CO)_9(\mu_3\text{-S})_2$ was examined at various sweep rates under two atmospheric conditions.

(i) The cyclic voltammograms measured under an argon atmosphere are shown in Figure 4. Four features in Figure 4 are noteworthy. First, the cathodic wave of $Fe_3(CO)_9(\mu_3\text{-S})_2$ in A diminished with increasing concentration of $P(OMe)_3$ in B and C. Second, the decrease in $Fe_3(CO)_9(\mu_3\text{-S})_2$ was compensated by a corresponding increase in the monosubstitution product $Fe_3(CO)_8(\mu_3\text{-S})_2[P(OMe)_3]$, as indicated by the fall in the cathodic wave of the reactant R and the rise in the CV wave of the product P. Third, the amount of R relative to P decreased with increasing scan rates at a given concentration of added $P(OMe)_3$. Fourth, at a set scan rate, the decrease in the ratio of R relative to P induced by added $P(OMe)_3$, as in B and C, ceased after more than 3 equiv of $P(OMe)_3$ was present as in D and E.

(ii) Similar changes in the cyclic voltammograms of $Fe_3(CO)_9(\mu_3\text{-S})_2$ were noted in the presence of added $P(OMe)_3$ when they were repeated under 1 atm of carbon monoxide. The most prominent difference was the reduced amount of ligand substitution observed at a given phosphite concentration and CV scan rate, as typically shown by the dotted curve in Figure 5. Essentially the same cyclic voltammogram could be obtained under a CO atmosphere as that observed under an argon atmosphere if compensated by a suitable increase in $P(OMe)_3$ concentration.

Discussion

The triiron carbonyl clusters $Fe_3(CO)_9(\mu_3\text{-E})_2$ (I) with the bridging cap E = NPh, PPh,[13] S, and Se form a series of isostructural analogues, is shown by the comparison of their relevant bond distances and angles listed in Table V.[28,40,41,43] These structural parameters together with those of related triiron clusters

(40) Wei, C. H.; Dahl, L. F. *Inorg. Chem.* **1965**, *4*, 493.
(41) Dahl, L. F.; Sutton, P. W. *Inorg. Chem.* **1963**, *2*, 1067.
(42) Schumann, H.; Magerstadt, M.; Pickardt, J. *J. Organomet. Chem.* **1986**, *240*, 407.
(43) Cook, S. L.; Evan, J.; Gray, L. R.; Webster, M. *J. Organomet. Chem.* **1982**, *236*, 367.

Table V. Pertinent Bond Distances and Angles in Triiron Clusters $Fe_3(CO)_9(\mu_3\text{-}E)_2$ with E = S, Se, Te, NPh, PPh, and AsPh

dist, Å (av)	S[a]	Se[b]	Te[c]	NMe(Ph)[d]	PPh[e]	AsPh[f]
Fe1–Fe2 (a)	2.60	2.64	2.75	2.49 (2.48)	2.71	2.77
Fe–E (b)	2.23	2.34	2.53	1.94 (1.94)	2.22	2.32
Fe1····Fe3	3.37	3.51	3.78	3.05 (3.08)	3.54	3.70

angles, deg (av)	S[a]	Se[b]	Te[c]	NMe(Ph)[d]	PPh[e]	AsPh[f]
Fe1–Fe2–Fe3 (θ_1)	81		87	76 (78)	81	84
Fe1–E–Fe2 (θ_2)	72	68	65	80 (78)	76	72
Fe1–E–Fe3 (θ_3)	98	97	96	105 (105)	107	105

[a] Reference 40. [b] Reference 41. [c] Reference 42. [d] Reference 28 (values in parentheses, this work). [e] Reference 43. [f] Reference 44.
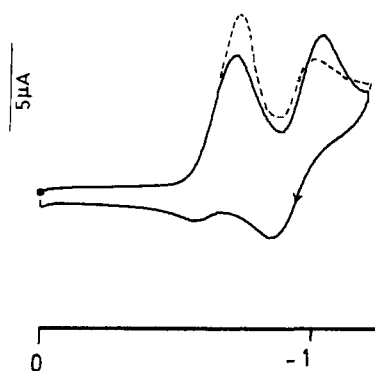

Figure 5. Typical change in the cyclic voltammograms of 5×10^{-3} M $Fe_3(CO)_9(\mu_3\text{-}S)_2$ and 2×10^{-2} M $P(OMe)_3$ in dichloromethane containing 0.1 M TBAP when an argon atmosphere (—) is replaced by a carbon monoxide atmosphere (···).

with E = Te and AsPh[42,44] constitute a regular trend with increasing atomic numbers for both the group V and VI (group 15 and 16) elements.[62] We conclude that the triiron clusters with E = S, Se, NPh, and PPh cannot be easily distinguished from each other on the basis of the effect of the bridging cap on the molecular structure.

It is noteworthy that the series of $Fe_3(CO)_9(\mu_3\text{-}E)_2$ all undergo ETC ligand substitution at rates that are substantially faster than those obtained thermally[21,22] in the absence of reductive stimulation. More importantly, it is readily apparent from our electrochemical experiments that the facility with which each triiron cluster undergoes ETC catalysis of ligand substitution is highly dependent on the nature of the briding cap E. In order to quantitatively assess the rate enhancement of the ETC process, it is necessary first to identify the rate-limiting step in the catalytic sequence. To do so, we note that the course of ETC ligand substitution is critically dependent on the initial electrode potential, as exemplified by the comparison of the stoichiometries observed in eq 4 and 5. Indeed, the electrode potentials required for monosubstitution correspond to the values of E^0 in Table IV appropriate for the reduction of the parent triiron cluster I to its anion radical, according to eq 6. Likewise the electrode potentials required for disubstitution correspond to the 1-electron reduction of the monosubstituted precursor, i.e. eq 8.
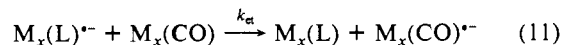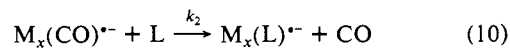
$$Fe_3(CO)_8(\mu_3\text{-}E)_2[P(OMe)_3] +$$
$$e^- \overset{E^0}{\rightleftharpoons} Fe_3(CO)_8(\mu_3\text{-}E)_2[P(OMe)_3]^{\bullet -} \quad (8)$$
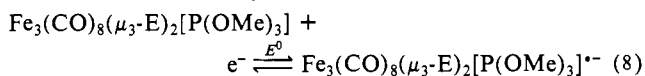
I. Mechanism of ETC Catalysis for Ligand Substitution of Metal Carbonyls. The importance of ETC catalysis for the ac-

tivation of these polynuclear clusters thus lies in the efficiency and selectivity with which multiple processes such as ligand substitution can be carried out under mild conditions. In the earlier study, Darchen and co-workers found the electrocatalysis of ligand substitution of the sulfur-bridged triiron cluster $Fe_3(CO)_8(\mu_3\text{-}S)_2G$ (where G = carbene) to occur efficiently on the millisecond time scale, as shown by the alteration of the cyclic voltammogram in the presence of added $P(OMe)_3$.[6] The detailed analysis of the heterogeneous electrode kinetics associated with the cyclic voltammetry of such an electrocatalytic process[45,46] establishes the general mechanism of the chain process for any metal carbonyl $M_x(CO)$ to consist of (a) the initiation step in eq 9 followed by

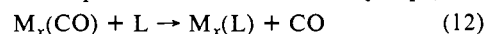$$M_x(CO) + e^- \overset{E^0}{\rightleftharpoons} M_x(CO)^{\bullet -} \quad (9)$$
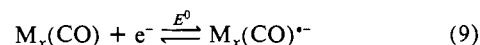
(b) the catalytic cycle in Scheme II, which leads to the overall

Scheme II

$$M_x(CO)^{\bullet -} + L \overset{k_2}{\longrightarrow} M_x(L)^{\bullet -} + CO \quad (10)$$

$$M_x(L)^{\bullet -} + M_x(CO) \overset{k_{et}}{\longrightarrow} M_x(L) + M_x(CO)^{\bullet -} \quad (11)$$

ligand substitution in eq 12. Since the initiation step (eq 9) and

$$M_x(CO) + L \rightarrow M_x(L) + CO \quad (12)$$

the driving force for electron transfer (eq 11) pose no kinetic limitiation,[47] the viability of the catalytic process lies in the susceptibility of the anion radical to ligand substitution in eq 10. The same basic mechanism applies to ETC catalysis of metal carbonyls that are activated by oxidation, i.e. eq 13, and in this case the labile species is the cation radical.[46]

$$M_x(CO) \overset{-E^0}{\rightleftharpoons} M_x(CO)^{\bullet +} + e^- \quad (13)$$
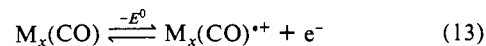
II. Rate Constants for the Triiron Carbonyl Clusters Fe_3-$(CO)_9(\mu_3\text{-}E)_2$ with E = S, Se, and NPh. In order to determine whether the general mechanism outlined in eq 9–11 also applies specifically to the series of triiron clusters I with E = S, Se, and NPh, we carried out a detailed analysis of the cyclic voltammetric behavior of the anion radical of the sulfur analogue as it was formed under the conditions in Figure 4. Indeed, the inspection of Figure 4 shows that the evolutionary change of the cyclic voltammograms ceases when the added $P(OMe)_3$ is more than 3 times greater than $Fe_3(CO)_9(\mu_3\text{-}S)_2$ (compare part C with parts D and E of Figure 1 at all sweep rates). Such a CV behavior indicates that the formation of the substitution product (identified as P in Figure 4) is not dependent on $P(OMe)_3$ at these higher

(44) Huttner, G.; Mohr, G.; Frank, A.; Schubert, U. *J. Organomet. Chem.* **1976**, *118*, C73.

(45) (a) Garreau, D.; Saveant, J. M. *J. Electroanal. Chem.* **1972**, *35*, 309; **1974**, *50*, 1. (b) Saveant, J. M.; Thiebault, A. *J. Electroanal. Chem. Interfacial Electrochem.* **1979**, *103*, 303.

(46) (a) Hershberger, J. W.; Klingler, R. J.; Kochi, J. K. *J. Am. Chem. Soc.* **1983**, *105*, 61. (b) Zizelman, P. M.; Amatore, C.; Kochi, J. K. *J. Am. Chem. Soc.* **1984**, *106*, 3771. (c) Hershberger, J. W.; Amatore, C.; Kochi, J. K. *J. Organomet. Chem.* **1983**, *250*, 345.

(47) See differences in E^0 in Table IV and the discussion by: Klingler, R. J.; Kochi, J. K. *J. Am. Chem. Soc.* **1981**, *103*, 2147; *J. Am. Chem. Soc.* **1982**, *104*, 4186.

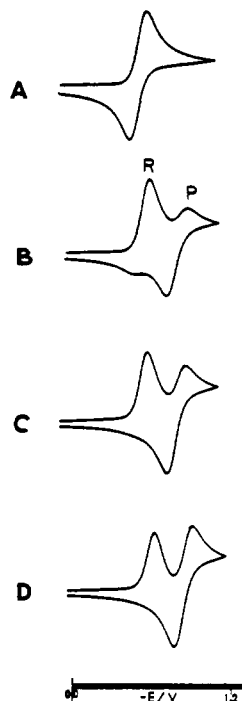**Figure 6.** Digital simulation of the cyclic voltammograms of $Fe_3(CO)_9(\mu_3\text{-}S)_2$ in the presence of $P(OMe)_3$ as a function of the operational rate constant. $k_2' = 0$, (A), 35 (B), 70 (C), and 140 M^{-1} s^{-1} (D) at 200 mV s^{-1}.

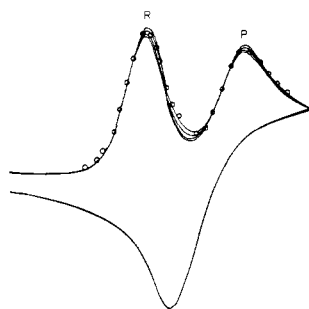**Figure 7.** Computer-generated cyclic voltammograms for operational rate constants k_2' (top to bottom) of 24, 27, 30, and 32 M^{-1} s^{-1}. Circles represent the cathodic data from the experimental cyclic voltammogram obtained for 4×10^{-3} M $Fe_3(CO)_9(\mu_3\text{-}S)_2$ and 7×10^{-2} M $P(OMe)_3$ at 200 mV s^{-1} in dichloromethane containing 0.2 M TBAP.

concentrations. The rate-limiting dissociation of a carbonyl ligand from the anion radical with the first-order rate constant k_1 in Scheme III accords with this conclusion. In other words, the

Scheme III

$$M_x(CO)^{\cdot-} \xrightarrow{k_1} M_x^{\cdot-} + CO \qquad (14)$$

$$M_x^{\cdot-} + L \xrightarrow{fast} M_x(L)^{\cdot-} \qquad (15)$$
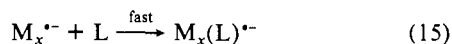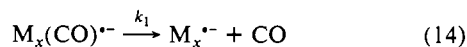
associative mechanism with the second-order rate constant k_2 for the ligand substitution of the anion radical $M(CO)^{\cdot-}$ in eq 10 (Scheme III) can be replaced with a stoichiometrically equivalent dissociative mechanism with the first-order rate constant k_1 in Scheme III. In order to test this formulation, we carried out the computer simulation of the series of cyclic voltammograms obtained at various concentrations of $P(OMe)_3$. The digital simulation of the cyclic voltammograms for Scheme II utilizes the method of finite differences as described by Feldberg.[48] Accurate simulation proceeds from a knowledge of E^0 for the redox couples

---

(48) (a) Feldberg, S. W.; Jeftic, L. *J. Phys. Chem.* **1971**, *75*, 2381. (b) Feldberg, S. W.; Jeftic, L. *J. Phys. Chem.* **1972**, *76*, 243. (c) Hawley, M. D.; Feldberg, S. W. *J. Phys. Chem.* **1966**, *70*, 3459.

Table VI. Determination of the Second-Order Rate Constant k_2' from the Digital Simulation of the Cyclic Voltammogram of $Fe_3(CO)_9(\mu_3\text{-}E)_2$ in the Presence of $P(OMe)_3$[a]

triiron cluster (concn, 10^3 M)	$P(OMe)_3$, M	k_2', M^{-1} s^{-1}	$k_2'[P(OMe)_3]$, s^{-1}
$Fe_3(CO)_9S_2$ 6.4	0.0174	380[b]	6.6
	0.0334	220[b]	7.3
	0.0606	100[b]	6.1
$Fe_3(CO)_9Se_2$ 4.7	0.019	45[c]	0.86
	0.053	20[c]	1.1
$Fe_3(CO)_9(NPh)_2$ 5.9	0.022	1.3×10^5 [d]	3×10^3 [e]

[a] In dichloromethane containing 0.1 M TBAP at 25 °C under an argon atmosphere. [b] At $V = 1$ V s^{-1}. [c] At $V = 200$ mV s^{-1}. [d] Estimated from relative peak currents at 500 V s^{-1} under a CO atmosphere, see text. [e] From the application of Scheme III.
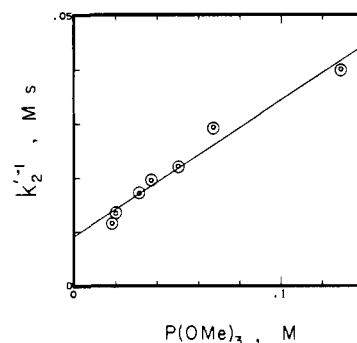

Figure 8. Evaluation of the rate constant k_1 for CO loss from the anion radical of $Fe_3(CO)_9(\mu_3\text{-}S)_2$ under a CO atmosphere. Digital simulations are based on the cyclic voltammograms from 5×10^{-3} M $Fe_3(CO)_9$-$(\mu_3\text{-}S)_2$ in dichloromethane containing 0.2 M TBAP and $(2-13) \times 10^{-2}$ M $P(OMe)_3$ at 200 mV s^{-1}.

in eq 11 as well as their intrinsic hetereogeneous rate constants k_s, the transfer coefficient α, and the diffusion constants D, as described in the Experimental Section. Thus our immediate goal is to substantiate the kinetic form of Scheme II and to determine an *operational* second-order rate constant k_2' for eq 10, i.e. eq 16, under conditions extant in the CV experiment. Following our
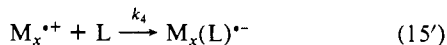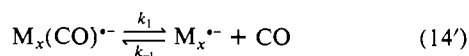
$$M_x(CO)^{\cdot-} + L \xrightarrow{k_2'} M_x(L)^{\cdot-} + CO \qquad (16)$$
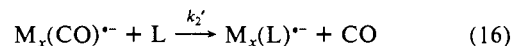
earlier observation, the electron-transfer step (eq 11) was taken to be rapid, with $k_{et} > 10^4$ M^{-1} s^{-1}.[49] The series of digital simulations of the cyclic voltammograms shown in Figure 6 were generated by systematically varying the value of k_2' for eq 16. Indeed, the successive diminution of the reactant curve R and the growth of the product wave P follow the same trend established by the experimental cyclic voltammograms in Figure 4A–C. The fit of the computer-generated cyclic voltammogram to the experimental curve in Figure 4C is illustrated in Figure 7. The sensitivity of the simulation method is shown by the locus of experimental points about the family of cyclic voltammograms generated by minor variations (±10%) in the value of k_2'. Table VI lists k_2', which was determined in this manner at various concentrations of added $P(OMe)_3$ such that the concentration ratio $[P(OMe)_3/[Fe_3(CO)_9(\mu_3\text{-}S)_2] \geq 3$. It is particularly noteworthy that, at these limiting $P(OMe)_3$ concentrations, the value of $k_2'[P(OMe)_3]$ is constant, as indicated by the last column in Table VI. It follows from the comparison of eq 16 with eq 14 and 15 (Scheme III) that $k_2'[P(OMe)_3]$ is equivalent to k_1 for Fe_3-$(CO)_9(\mu_3\text{-}S)_2$ under these conditions. The value of k_1 indicated for the selenium analogue by the same procedure is also included in Table VI.

The magnitude of the dissociation rate constant k_1 can also be evaluated from CV experiments carried out under an atmosphere of carbon monoxide (compare Figure 5). Under these conditions, Scheme III must be modified slightly to include the mass action effect of CO on the anion radical, i.e. Scheme IV. The general

---

(49) See discussion in ref 46.

Scheme IV

$$M_x(CO)^{\bullet -} \underset{k_{-1}}{\overset{k_1}{\rightleftharpoons}} M_x^{\bullet -} + CO \qquad (14')$$

$$M_x^{\bullet +} + L \xrightarrow{k_4} M_x(L)^{\bullet -} \qquad (15')$$

rate law for the disappearance of the anion radical according to Scheme IV is given in eq 17, as presented in the Experimental

$$-\frac{d[M_x(CO)^{\bullet -}]}{dt} = \frac{k_1 k_4 [M_x(CO)^{\bullet -}][L]}{k_{-1}[CO] + k_4[L]} \qquad (17)$$

Section. The relationship of this rate expression with the operational second-order rate process given in eq 16 is then eq 18. In

$$1/k_2' = k_{-1}[CO]/k_1 k_4 + [L]/k_1 \qquad (18)$$

accord with this relationship, the plot of $k_2'^{-1}$ obtained by digital simulation (vide supra) of cyclic voltammograms under a CO atmosphere as a function of the concentration of $P(OMe)_3$ is found to be linear in Figure 8. The value of $k_1 = 4\ s^{-1}$ evaluated from the slope in Figure 8 is in reasonable agreement with the value in Table VI obtained under an argon atmosphere by the application of the first-order mechanism in Scheme III. These results thus establish the rate-limiting process in the ETC catalysis of ligand substitution of the sulfur analogue to be CO dissociation from the anion radical $Fe_3(CO)_9(\mu_3\text{-}S)_2^{\bullet -}$ in eq 14.

The nitrogen analogues $Fe_3(CO)_9(\mu_3\text{-}NPh)_2$ and $Fe_3(CO)_9$-$(\mu_3\text{-}NC_6H_4\text{-}p\text{-}OMe)_2$[50] both undergo ETC catalysis of ligand substitution with substantially greater facility than the sulfur and selenium analogues. Thus, Figure 3 shows that the anion radicals of $Fe_3(CO)_9(\mu_3\text{-}NPh)_2$ are highly labile, and substantial amounts of disubstitution are observed during the CV experiment (see Figure 3B). This complication can be circumvented in two ways—by increasing the CV scan rate and/or by introducing a CO atmosphere. Thus the cyclic voltammogram of 6×10^{-3} M $Fe_3(CO)_9(\mu_3\text{-}NPh)_2$ and 2×10^{-2} M $P(OMe)_3$ in dichloromethane carried out under an atmosphere of carbon monoxide at a sweep rate of 500 V s^{-1} showed the evolution of only the monosubstituted product. Under these conditions, the concomitant diminution of the initial cathodic peak current i_{po}^R of $Fe_3(CO)_9(\mu_3\text{-}NPh)_2$ corresponded to $i_{po}^R/i_p^R = 0.71$. Digital simulation of the cyclic voltammogram based on the procedure described above for Scheme II can be achieved with an operational rate constant k_2' $= 1 \times 10^5$ M^{-1} s^{-1}. If it is assumed that ligand substitution of $Fe_3(CO)_9(\mu_3\text{-}NPh)_2^{\bullet -}$ occurs by the same first-order process as that for the sulfur analogue in Scheme III, the disssociation rate constant of $k_1 \cong 3 \times 10^3$ s^{-1} is obtained.

III. Competitive Rates and Mechanism of ETC Catalysis for Triiron Clusters with Sulfene, Selenene, Nitrene, and Phosphinidene Bridging Caps. The facile ligand substitution of the series of triiron carbonyl clusters I by ETC catalysis derives from the enhanced lability of the anion radical $Fe_3(CO)_9(\mu_3\text{-}E)_2^{\bullet -}$, which is common to all the members with E = S, Se, NPh, and PPh.[13] However, our results demonstrate that these anion radicals follow unique and distinctive pathways for ligand substitution. For example, the *rates* at which each triiron carbonyl anion radical suffers ligand substitution are highly differentiated by the nature of the bridging cap. At one extreme, the ETC catalysis of the phosphorus analogue occurs so slowly[13] that (a) the current efficiency is very low with the turnover number TN approaching unity, (b) every anion radical that is an intermediate can be separately observed and identified from its ESR spectrum, and (c) the transient cyclic voltammograms simply consist of the superpositions of those of the reactants and products. At the other extreme, the nitrogen analogue reacts so rapidly that (a) the current efficiency is very high with TN exceeding 600, (b) the intermediates are too unstable to be discerned, and (c) the transient cyclic voltammograms are highly convoluted even in the presence of small amounts of added ligand (compare Figure 3).

In order to present such diverse results within a single context, the relative rates of disappearance are estimated in Table VII at

(50) See also: LaHuerta, P.; LaTorre, J.; Sanau, M. *J. Organomet. Chem.* **1985**, *286*, C27.

Table VII. Effect of the Bridging Cap E on the Reactivity of the Anion Radicals of $Fe_3(CO)_9(\mu_3\text{-}E)_2^a$

E	Rate,[b] M s^{-1}	E	Rate,[b] M s^{-1}
S	4×10^{-3}	PPh	$1.2 \times 10^{-6\ c}$
Se	6×10^{-4}	NPh	2

^{a} In dichloromethane containing 0.2 M TBAP at 25 °C unless indicated otherwise. ^{b} From k_1 in the last column of Table VI times 5.8×10^{-4} M. ^{c} By direct measurement of 5.8×10^{-4} M $Fe_3(CO)_9(\mu_3\text{-}PPh)_2^{\bullet -}$ in THF from ref 13.

Table VIII. First-Order Rate Constants k_1 for Decomposition of the Anion Radicals $Fe_3(CO)_9(\mu_3\text{-}E)_2^{\bullet -\ a}$

E	k_1,[b] s^{-1}	E	k_1,[b] s^{-1}
S	6.6	PPh	$\sim 2 \times 10^{-3\ c}$
Se	1.0	NPh	$\sim 3 \times 10^3$

^{a} In dichloromethane containing 0.2 M TBAP at 25 °C unless indicated otherwise. ^{b} From the last in Table VI, with $k_2'[P(OMe)_3] = k_1$. ^{c} Estimated from the value in column 2, Table VII, divided by 5.8×10^{-4} M in THF.

the same *initial* concentration for the anion radical.[51] As may be expected, the reactivities of the sulfur and selenium analogues, as indicated by the rates in column 2, are not highly differentiated from each other. However, the difference between nitrene and phosphinidene analogues by a factor of almost 10^6 is too large to be accounted for as an element effect. Thus, the latter should be reflected in the reversible reduction potentials required to convert the triiron cluster to the corresponding anion radical. However, the results in Table IV show no trend of E^0 with either the rates in Table VII or the catalytic efficiency as measured by TN in Table I. Moreover, it is important to reemphasize that the difference in reactivity of the nitrene and sulfene analogues by a factor of 10^3 in ETC catalysis is completely unrelated to their reactivity in thermal reactions, which occur at similar rates.[21,22] Accordingly, the structure (Table V) and properties (Tables II and III) that are pertinent to the parent triiron clusters are not directly related to the reactive intermediates in ETC catalysis.

The difference in the rates of reactivity of the nitrene and phosphinidene analogues in ETC catalysis lies in the mechanism by which their anion radicals undergo ligand substitution in the slow rate-determining step (see eq 14, Scheme III). Thus, the analysis of the first-order rate constants k_1 in Table VIII is based on two different mechanisms. For example, the earlier study[13] of the phosphinidene analogue identified k_1 with the skeletal opening of the cluster $Fe_3(CO)_9(\mu_3\text{-}PPh)_2^{\bullet -}$ to expose a coordinatively unsaturated 17-electron iron center, i.e. eq 19. On the

$$(19)$$
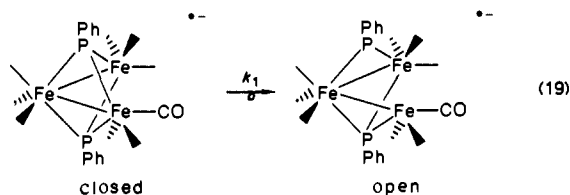
other hand, for the nitrene analogue, the results of this study focus on k_1 as the dissociative loss of a carbonyl ligands from Fe_3-$(CO)_9(\mu_3\text{-}NPh)_2^{\bullet -}$ to generate coordinative unsaturation at an iron site and maintain the cluster framework intact, i.e.[52] eq 20. It

$$+ CO \qquad (20)$$
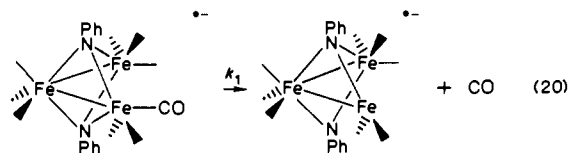
(51) Chosen as 5.8×10^{-4} M from ref 13.
(52) Although the rapidity of ETC catalysis of ligand substitution in the nitrogen analogue precluded a rigorous kinetic analysis of k_1 (vide supra), it is unlikely that it proceeds by the analogous mechanism to that of the phosphorus analogue in eq 19. Thus the strong retarding effect of CO is not easily reconciled with a rate-limiting opening on the cluster framework.

Electron-Transfer Activation of Triiron Clusters

J. Am. Chem. Soc., Vol. 109, No. 25, 1987 7733

is not clear at this juncture why the bridging caps induce these diverse pathways as a means to relieve electron supersaturation in the triiron cluster. The difference in electronegativity of nitrogen and phosphorus may be partly responsible. However, such a property can hardly account for the dissociative pathway analogous to that in eq 20 enjoyed by the sulfur and selenium analogues. Furthermore, the factor of more than 10^3, which separates the nitrogen analogue from the sulfur and selenium analogues (Table VIII), seems to be opposite to that expected solely from electronegativity considerations.[53,54]

The marked influence of the bridging cap E on the ETC behavior of $Fe_3(CO)_9(\mu_3\text{-}E)_2$ is undoubtedly related to the nature of the bonding in the labile anion-radical intermediates. Although this structural problem must be ultimately resolved by theoretical analysis of such open-shelled clusters, the mechanistic distinction can be viewed in two interrelated ways. First, the relative magnitudes of the first-order rate constants for the anion radicals in Table VIII emphasize the exceptionally slow rate of CO loss from $Fe_3(CO)_9(\mu_3\text{-}PPh)_2^{\bullet-}$ relative to the others. As a result, the phosphinidene anion radical relieves electron supersaturation in the cluster by scission of an iron bond from the capping ligand. The same pathway could pertain with nitrogen, sulfur, and selenium analogues if CO dissociation from their anion radicals were slower. The central question then resolves to either why CO loss from $Fe_3(CO)_9(\mu_3\text{-}PPh)_2^{\bullet-}$ is so slow or, equivalently, why CO loss from the other anion radicals is so fast. Second, the bonding in the cluster anion radicals can be viewed in at least two extreme valence bond (VB) structures, which emphasize either metal–metal interactions or metal–ligand interactions to maintain the cluster anion radical intact. If so, the activation of the phosphinidene cluster according to eq 19 could be associated with VB structure in the anion radical with a weak metal–ligand bond. By the same token, the activation of the nitrogen, sulfur, and selenium clusters according to eq 20 could be associated with VB structure in the anion radical with strong metal–ligand bonds.[55] The ^{31}P hyperfine splittings observed in the ESR spectrum[23] of $Fe_3(CO)_9(\mu_3\text{-}PPh)_2^{\bullet-}$ indeed accord with the occupation of the LUMO located about the phosphinidene cap as expected from the former. Unfortunately, the highly transient character of the nitrogen, sulfur, and selenium analogues as yet precludes similar ESR measurements of their anion radicals for comparative purposes.[39,56]

Summary and Conclusions

The series of triiron clusters $Fe_3(CO)_9(\mu_3\text{-}E)_2$ with bridging caps E = S, Se, NPh, and PPh are all effectively activated by ETC catalysis of ligand substitution. The rate, efficiency, and selectivity of ETC catalysis are strongly modulated by the nature of the bridging cap. The quantitative analysis of the ETC kinetics by digital simulation of the cyclic voltammograms of the sulfur and selenium analogues identifies the rate-limiting step with the anion radical $Fe_3(CO)_9(\mu_3\text{-}E)_2^{\bullet-}$ as the reactive intermediate. The marked difference between the anion radicals of the phosphorus and nitrogen (sulfur or selenium) clusters lies in the pathways by which they undergo first-order reaction according to eq 19 and 20, respectively. Such a mechanistic distinction between nitrogen and phosphorus clusters is not apparent from the experimental observations on the basis of their molecular structures or their redox properties. The latter encourages the further theoretical

analysis of the bonding in this series of isostructural transition-metal clusters.

Experimental Section

Materials. The sulfur and selenium analogues of the triiron carbonyl clusters $Fe_3(CO)_9(\mu_3\text{-}S)_2$ and $Fe_3(CO)_9(\mu_3\text{-}Se)_2$, respectively, were prepared by the method of Hieber and Gruber.[24] The nitrogen clusters $Fe_3(CO)_9(\mu_3\text{-}NC_6H_5)_2$ and $Fe_3(CO)_9(\mu_3\text{-}NC_6H_4\text{-}p\text{-}OCH_3)_2$ were synthesized from the reduction of nitrobenzene and p-nitroanisole by $Fe_3(CO)_{12}$ according to Landesberg and co-workers.[25] They were purified by column chromatography over silica gel (Grace, Davisil-62) followed by recrystallization from n-pentane. Trimethyl phosphite (Victor Chemical) was purified by distillation from sodium under an argon atmosphere. The supporting electrolyte tetra-n-butylammonium perchlorate (TBAP, G. F. Smith Co.) was crystallized twice from a mixture of ethyl acetate and hexane. It was recrystallized from ethyl acetate and dried in vacuo.

Instrumentation. Infrared spectra were recorded on a Nicolet DX 10 FT spectrometer. A JEOL FX-90Q FT spectrometer was used to measure the ^1H and ^{31}P NMR spectra at operating frequencies of 89.55 and 36.23 MHz, respectively. Cyclic voltammograms at conventional scan rates (0.1–10 V s^{-1}) were obtained with platinum disk electrodes using an ir-compensated potentiostat[45a] driven by a Princeton Applied Research (PAR) Model 175 universal programmer.[38] Cyclic voltammetric experiments at fast scan rates (500 and 10000 V s^{-1}) were performed at platinum microelectrodes with a potentiostat designed by Howell and Wightman[57] interfaced to a Gould Biomation Model 4500 waveform digitizer with 10-ns access time resolution. Potentials were referenced to SCE in contact with the anolyte through a cracked glass tip and calibrated with ferrocene.[36] Bulk electrolyses and coulometry were performed on a PAR Model 173 potentiostat equipped with a PAR Model 163 coulometer with an air-tight and grease-free cell.[38] All coulometric experiments were performed at constant potential under an argon atmosphere, and they were followed by periodically measuring the cyclic voltammogram in situ or extracting an aliquot of the catholyte for IR and/or TLC analysis.

Synthesis of $Fe_3(CO)_8(\mu_3\text{-}NPh)_2[P(OMe)_3]$. A three-chambered electrolysis cell filled with argon was charged with 0.23 g (0.38 mmol) of the nitrene cluster $Fe_3(CO)_9(\mu_3\text{-}NPh)_2$ and 0.10 mL (0.85 mmol) of trimethyl phosphite in 20 mL of THF containing 0.2 M TBAP. Cathodic current at constant potential of −0.82 V was passed through the solution. The course of reaction was followed by the periodic removal of aliquots of the catholyte for IR and TLC analysis. When the high-frequency carbonyl band at 2086 cm^{-1} in the IR spectrum was no longer visible (~ 2 min), the passage of current was terminated. For the coulometry, see Table I. The reaction mixture was chromatographed on silica gel with hexane as the eluent. Removal of the solvent yielded 0.18 g (68%) of dark purple crystals. Anal. Calcd for $C_{23}H_{19}Fe_3N_2O_{11}P$: C, 39.58; H, 2.74. Found: C, 39.46; H, 2.80.[58]

Synthesis of $Fe_3(CO)_7(\mu_3\text{-}NPh)_2[P(OMe)_3]_2$. The monosubstituted nitrogen cluster $Fe_3(CO)_8(\mu_3\text{-}NPh)_2[P(OMe)_3]$ (0.13 g, 0.19 mmol) and trimethyl phosphite (0.05 mL, 0.42 mmol) were dissolved in 20 mL of THF containing 0.2 M TBAP. The solution was reduced potentiostatically at −0.95 V until the IR band at 2066 cm^{-1} of the reactant disappeared completely (~ 30 min). The reaction mixture was chromatographed on a silica gel column with 4:1 v/v mixture of hexane and benzene to yield 0.083 g (56%) of $Fe_3(CO)_7(\mu_3\text{-}NPh)_2[P(OMe)_3]_2$. Anal. Calcd for $C_{25}H_{28}Fe_3N_2P_2O_{13}$: C, 37.82; H, 3.55. Found: C, 37.76; H, 3.59.

Synthesis of $Fe_3(CO)_8(\mu_3\text{-}Se)_2[P(OMe)_3]$. Electrochemical reduction of a mixture consisting of 0.15 g (0.26 mmol) of $Fe_3(CO)_9(\mu_3\text{-}Se)_2$ and 0.10 mL (0.83 mmol) of trimethyl phosphite in 20 mL of THF containing 0.2 M TBAP was effected at a constant potential of −0.55 V for ~ 20 min. Workup of the reaction mixture as described above yielded 0.095 g (54%) of $Fe_3(CO)_8(\mu_3\text{-}Se)_2[P(OMe)_3]$. The ^1H and ^{31}P NMR spectra of $Fe_3(CO)_8(\mu_3\text{-}Se)_2[P(OMe)_3]$ and of the related sulfur cluster (vide infra) consisted of a mixture of isomers. The $^{31}P\{^1H\}$ NMR spectrum for each cluster at −59 °C showed two resonances (Table III). As the temperature was raised, the upfield resonance remained sharp but the downfield resonance began to show signs of coalescence, as shown in Figure 9 for $Fe_3(CO)_8(\mu_3\text{-}Se)_2[P(OMe)_3]$. The attendant changes in chemical shifts were as follows: (temperature, δ): 25 °C, 168.7, 171.3; 0 °C, 169.1, 172.6; −22 °C, 169.3, 173.6; −48 °C, 169.7, 176.0; −59 °C, 169.7, 175.9. The sharp upfield resonance was tentatively assigned to the monophosphite substituted at the apical Fe2 position to accord with the earlier ^{13}C NMR study.[30] The broad downfield resonance was attributed to the monophosphite substituted at a basal Fe1, owing to line

(53) It is also opposite to the order of the trans effect. See: Cotton, F. A.; Wilkinson, G. *Advanced Inorganic Chemistry*, 4th ed.; Wiley: New York, 1980.

(54) Note also that the nitrogen analogue leads specifically to basal substitution whereas the sulfur and selenium analogues lead to both basal (predominant) as well as apical substitution.

(55) This suggestion for the difference between nitrene and phosphinidene runs counter to experimental observations in the anion radicals of *mononuclear* carbonyls. Thus the 19-electron $Mn(CO)_5NCMe$ and $Mn(CO)_5py$ produced in the electrochemical reduction of $Mn(CO)_5NCMe^+$ and $Mn(CO)_5py^+$, respectively, undergo exclusive loss of the nitrogen-centered ligands MeCN and py.[38] On the other hand, in a series of phosphite- and phosphine-substituted 19-electron $Mn(CO)_5P$, CO loss is competitive with loss of P.

(56) A synthesis of bicapped triiron clusters with hetero bridges such as $Fe_3(CO)_9(\mu_3\text{-}PPh)(\mu_3\text{-}NPh)$ may ultimately offer an entry into the solution of these interesting problems.

(57) Howell, J. O.; Wightman, R. M. *Anal. Chem.* **1984**, *56*, 524.

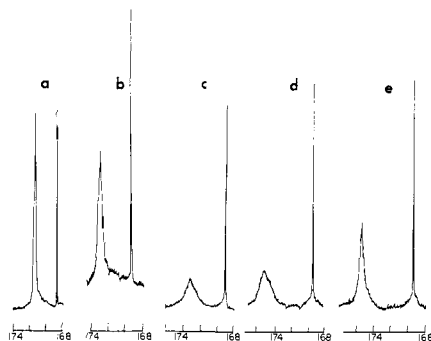(58) All elemental microanalyses by Atlantic Microlabs, Atlanta, GA.

Figure 9. Temperature-dependent $^{31}P\{^{1}H\}$ NMR spectrum of Fe$_3$-(CO)$_8$(μ_3-Se)$_2$[P(OMe)$_3$] at (a) 25, (b) 0 (higher gain), (c) −21, (D) −48, and (e) −59 °C in chloroform-d.

broadening from the equatorial–axial conformational change similar to that observed earlier by Muetterties and co-workers.[19c]

Synthesis of Fe$_3$(CO)$_7$(μ_3-Se)$_2$[P(OMe)$_3$]$_2$. The selenium cluster Fe$_3$(CO)$_9$(μ_3-Se)$_2$ (0.26 g, 0.46 mmol) and 0.25 mL (2.3 mmol) of trimethyl phosphite in 20 mL of THF containing 0.2 M TBAP were initially reduced at a constant potential of −0.60 V until the IR analysis indicated that the high-energy carbonyl band at 2090 cm^{-1} was·gone (∼20 min). At this point, the potential was increased to −0.90 V until the high-energy band at 2070 cm^{-1} of the monosubstituted phosphite had disappeared (∼25 min). Chromatographic workup, in the manner described above, yielded 0.19 g (63%) of Fe$_3$(CO)$_7$(μ_3-Se)$_2$[P(OMe)$_3$]$_2$.

Synthesis of Fe$_3$(CO)$_8$(μ_3-S)$_2$[P(OMe)$_3$]. An argon-filled three-chambered electrolysis cell was charged with 0.18 g (0.37 mmol) of Fe$_3$(CO)$_9$(μ_3-S)$_2$, 0.2 mL (1.67 mmol) of P(OMe)$_3$, and 20 mL of THF containing 0.2 M TBAP. Cathodic current at a constant potential of −0.55 V was passed through the solution in increments corresponding to 0.5% reduction. The extent of reaction was monitored by the periodic extraction of aliquots for thin-layer chromatography and IR spectroscopy. Reduction was terminated when the high-frequency carbonyl band at 2093 cm^{-1} in the IR spectrum could no longer be detected (∼20 min). The reaction mixture was passed through a silica gel column with n-hexane as the eluent. Fe$_3$(CO)$_8$(μ_3-S)$_2$[P(OMe)$_3$] was isolated as a dark red oil, which subsequently solidified when placed in vacuo; yield 0.14 g (65%). The ^{31}P NMR spectrum of Fe$_3$(CO)$_8$(μ_3-S)$_2$[P(OMe)$_3$] (Table III) was similar to that of the selenium analogue (vide supra), from which we deduced that a similar mixture of basal and apical isomers were present. For the sulfur analogue Fe$_3$(CO)$_8$(μ_3-S)$_2$[P(OMe)$_3$], the temperature-dependent changes in the chemical shifts of the pair of doublets in the $^{31}P\{^{1}H\}$ NMR spectrum were the following: 25 °C, 165.1, 168.8; −36 °C, 165.6, 170.0; −59 °C, 166.3, 172.9.

Synthesis of Fe$_3$(CO)$_7$(μ_3-S)$_2$[P(OMe)$_3$]$_2$. Fe$_3$(CO)$_8$(μ_3-S)$_2$[P(OMe)$_3$] (0.165 g, 0.28 mmol) obtained above was reduced at −0.80 V in the presence of 0.10 mL (0.83 mmol) of trimethyl phosphite in 20 mL of THF containing 0.20 M TBAP as described earlier. Upon the disappearance of the high-energy band at 2070 cm^{-1} in ∼20 min, the catholyte was worked up as described above to yield 0.086 g (45%) of Fe$_3$(CO)$_7$-(μ_3-S)$_2$[P(OMe)$_3$]$_2$.

Thermal Reactions of Fe$_3$(CO)$_9$(μ_3-E)$_2$ with Trimethyl Phosphite. For comparison with the ETC catalysis of ligand substitution as described above, a parallel set of control experiments was carried out without electrostimulation. In a typical experiment, a THF solution of the triiron cluster, trimethyl phosphite, and TBAP in equivalent concentrations as those given above was allowed to stand at 25 °C in the dark. An aliquot of the mixture was periodically extracted for IR and TLC analysis. The concentrations of all the triiron clusters remained unchanged for at least 2 h. The IR bands of the products of the chalcogen clusters became perceptible only after 3 h.

Kinetics Data from Cyclic Voltammetric Experiments. Cyclic voltammograms were typically obtained under either an argon or a CO atmosphere from (2–8) × 10^{-3} M solutions of the triiron cluster in either dichloromethane or tetrahydrofuran containing 0.1 M TBAP and variable amounts of trimethyl phosphite (usually in the range of (1–30) × 10^{-3} M). The experimental points (as in Figure 7) were obtained by subtraction of the background charging current from each experimental point. Only the initial cathodic scan was simulated, owing to the slight complications from the second disubstitution (compare Figure 3).

The digital simulation of the cyclic voltammograms was based on the method of Feldberg.[59] The heterogeneous rate constants k_s were obtained from solutions of the triiron cluster in the absence of P(OMe)$_3$ by

(59) Feldberg, S. W. *Electroanal. Chem.* **1969**, *3*, 199.

Table IX. Final Atomic Parameters for the Non-Hydrogen Atoms of an Independent Fe$_3$(CO)$_8$(μ_3-NPh)$_2$[P(OMe)$_3$] Molecule[a]

atom	x	y	z	B, Å^2
Fe1	0.60723 (8)	0.27362 (4)	0.16514 (4)	2.88 (2)
Fe2	0.59390 (8)	0.16934 (4)	0.07787 (4)	3.23 (2)
Fe3	0.37256 (8)	0.14997 (4)	0.16337 (4)	3.13 (2)
P	0.4958 (2)	0.32863 (8)	0.26017 (8)	3.32 (3)
O1	0.6691 (5)	0.4245 (2)	0.0921 (2)	6.7 (1)
O2	0.8958 (4)	0.2862 (2)	0.2233 (2)	5.8 (1)
O3	0.8509 (5)	0.2523 (3)	0.0079 (2)	7.6 (1)
O4	0.4552 (5)	0.1468 (3)	−0.0591 (2)	7.3 (1)
O5	0.7410 (6)	0.0185 (2)	0.0668 (3)	8.3 (1)
O6	0.1315 (4)	0.1257 (2)	0.0703 (2)	6.3 (1)
O7	0.3866 (5)	−0.0168 (2)	0.1930 (2)	6.6 (1)
O8	0.1754 (4)	0.1891 (2)	0.2968 (2)	5.8 (1)
O9	0.4661 (4)	0.2828 (2)	0.3385 (2)	4.25 (9)
O10	0.3350 (4)	0.3549 (2)	0.2458 (2)	4.51 (9)
O11	0.5857 (4)	0.4008 (2)	0.2777 (2)	4.9 (1)
N1	0.5722 (4)	0.1660 (2)	0.1883 (2)	2.80 (9)
N2	0.4410 (4)	0.2453 (2)	0.1133 (2)	2.76 (9)
C1	0.6409 (6)	0.3654 (3)	0.1188 (3)	3.9 (1)
C2	0.7831 (6)	0.2787 (3)	0.2009 (3)	3.8 (1)
C3	0.7490 (6)	0.2233 (3)	0.0394 (3)	4.7 (1)
C14	0.6544 (6)	0.0482 (3)	0.3571 (3)	4.4 (1)*
C15	0.8030 (6)	0.0342 (3)	0.3428 (3)	4.6 (1)*
C16	0.8774 (6)	0.0612 (3)	0.2775 (3)	4.3 (1)*
C17	0.8030 (5)	0.1046 (3)	0.2256 (3)	3.5 (1)*
C18	0.3550 (5)	0.2987 (3)	0.0717 (3)	3.0 (1)*
C19	0.2092 (5)	0.3156 (3)	0.0960 (3)	3.2 (1)*
C20	0.1271 (6)	0.3703 (3)	0.0578 (3)	4.0 (1)*
C21	0.1917 (6)	0.4089 (3)	−0.0047 (3)	4.2 (1)*
C22	0.3345 (6)	0.3932 (3)	−0.0297 (3)	4.5 (1)*
C23	0.4190 (6)	0.3377 (3)	0.0066 (3)	3.9 (1)*
C4	0.5113 (6)	0.1570 (3)	−0.0063 (3)	4.5 (1)
C5	0.6850 (7)	0.0775 (3)	0.0717 (3)	5.1 (2)
C6	0.2242 (6)	0.1366 (3)	0.1062 (3)	4.0 (1)
C7	0.3796 (6)	0.0489 (3)	0.1830 (3)	4.1 (1)
C8	0.2539 (5)	0.1760 (3)	0.2451 (3)	3.7 (1)
C9	0.5844 (7)	0.2622 (3)	0.3830 (3)	5.7 (2)
C10	0.2163 (6)	0.3809 (4)	0.2980 (3)	5.8 (2)
C11	0.5496 (7)	0.4498 (4)	0.3379 (4)	6.5 (2)
C12	0.6510 (5)	0.1202 (3)	0.2390 (3)	2.9 (1)*
C13	0.5770 (6)	0.0916 (3)	0.3061 (3)	3.6 (1)*

[a] Anisotropically refined atoms are given in the form of the isotropic equivalent thermal parameter defined as $^{4}/_{3}[a^2B(1,1) + b^2B(2,2) + c^2B(3,3) + ab(\cos \gamma)B(1,2) + ac(\cos \beta)B(1,3) + bc(\cos \alpha)B(2,3)]$. Asterisks identify values for atoms refined isotropically.

simulating the peak to peak separation at various scan rates. The values for Fe$_3$(CO)$_9$S$_2$ of $k_s = 5 \times 10^{-3}$ cm^{-1} s^{-1}, for Fe$_3$(CO)$_9$Se$_2$ of $k_s = 3 \times 10^{-3}$ cm^{-1} s^{-1}, and for Fe$_3$(CO)$_9$(NPh)$_2$ of $k_s = 1.2 \times 10^{-3}$ cm^{-1} s^{-1} were used in the simulations. The homogeneous rate constant of $k_{et} = 10^4$ M^{-1} s^{-1} was used for the sulfur and selenium analogues, and 10^6 M^{-1} s^{-1} was used for the nitrogen analogues. The transfer coefficient was arbitrarily set at $\alpha = 0.5$ for each species, and the standard potentials of Fe$_3$(CO)$_9$S$_2$, Fe$_3$(CO)$_9$Se$_2$, and Fe$_3$(CO)$_9$(NPh)$_2$ were taken as E^0 = −0.61, −0.55, and −0.73 V, respectively. The heterogeneous rate constants for the products were taken to be the same as that of the reactant except for the sulfur analogue for which $k_s = 3 \times 10^{-3}$ cm^{-1} s^{-1} provided a better fit of the data. The standard potentials for the products from the sulfur, selenium, and nitrogen analogues were taken as E^0 = −0.865, −0.88, and −0.98 V, respectively. The diffusion constant was set at a single value of 2.5 × 10^{-5} cm^2 s^{-1} for all species.

For the kinetics in Scheme IV, pseudo steady state was taken for the coordinatively unsaturated anion radical, i.e.

$$d[\text{Fe}_3{}^{\cdot-}]/dt = k_1[\text{Fe}_3(\text{CO})^{\cdot-}] - k_{-1}[\text{Fe}_3{}^{\cdot-}][\text{CO}] - k_4[\text{Fe}_3{}^{\cdot-}][\text{L}] = 0$$

or

$$[\text{Fe}_3{}^{\cdot-}] = k_1[\text{Fe}_3(\text{CO})^{\cdot-}]/(k_{-1}[\text{CO}] + k_4[\text{L}])$$

The rate of formation of product is determined by the rate of ligand association in eq 15′, i.e. eq 21. The rate constant k_2' for the CV

$$\text{rate} = k_1 k_4[\text{Fe}_3(\text{CO})^{\cdot-}][\text{L}]/(k_{-1}[\text{CO}] + k_4[\text{L}]) \quad (21)$$

simulation is obtained from the relationship in eq 22. Equating eq 21 and 22 leads to eq 18.

$$\text{rate} = k_2'[\text{Fe}_3(\text{CO})^{\cdot-}][\text{L}] \quad (22)$$

Table X. Typical Bond Distances in Fe₃(CO)₈(μ₃-NPh)₂[P(OMe)₃]^a

atom 1	atom 2	dist, Å	atom 1	atom 2	dist, Å
Fe1	Fe2	2.478 (1)	O4	C4	1.146 (4)
Fe1	P	2.151 (1)	O5	C5	1.138 (4)
Fe1	N1	1.935 (2)	O6	C6	1.137 (3)
Fe1	N2	1.939 (2)	O7	C7	1.153 (3)
Fe1	C1	1.790 (4)	O8	C8	1.141 (3)
Fe1	C2	1.785 (4)	O9	C9	1.429 (4)
Fe2	Fe3	2.423 (1)	O10	C10	1.434 (4)
Fe2	N1	1.975 (2)	N1	N2	2.281 (3)
Fe2	N2	1.972 (2)	O11	C11	1.420 (4)
Fe2	C3	1.777 (4)	N1	C12	1.416 (3)
Fe2	C4	1.781 (4)	N2	C18	1.429 (3)
Fe2	C5	1.788 (4)	C12	C13	1.398 (4)
Fe3	N1	1.939 (2)	C12	C17	1.396 (4)
Fe3	N2	1.941 (2)	C13	C14	1.392 (4)
Fe3	C4	1.801 (4)	C14	C15	1.364 (4)
Fe1	Fe3	3.079 (1)	C15	C16	1.364 (4)
Fe3	C7	1.785 (4)	C16	C17	1.388 (4)
Fe3	C8	1.802 (4)	C18	C19	1.378 (4)
P	O9	1.588 (2)	C18	C23	1.407 (4)
P	O10	1.558 (2)	C19	C20	1.391 (4)
P	O11	1.583 (2)	C20	C21	1.369 (4)
O1	C1	1.140 (3)	C21	C22	1.352 (4)
O2	C2	1.148 (3)	C22	C23	1.395 (4)
O3	C3	1.150 (4)			

^{a} Numbers in parentheses are estimated standard deviations in the least significant digits.

The kinetics under an atmosphere of CO shown in Figure 8 was obtained by CV simulation for [P(OMe)₃] (10⁻³ M) and k_2' (M⁻¹ s⁻¹): 18.2, 68; 20.0, 74; 31.3, 58; 37.0, 51; 50.1, 45; 67.0, 34; 129, 25.

X-ray Crystallography of Fe₃(CO)₈(μ₃-NPh)₂[P(OMe)₃]. A large red-black slab having dimensions 0.60 × 0.35 × 0.15 mm was mounted on a glass fiber in a random orientation on an Enraf-Nonius CAD-4 automatic diffractometer. The radiation used was Mo Kα monochromatized by a dense graphite crystal assumed for all purposes to be 50% imperfect. Final cell constants, as well as other information pertinent to data collection and refinement were the following: space group, P1̄, triclinic; a = 9.065 (2), b = 17.474 (8), c = 17.989 (6) Å; $α$ = 87.11 (4), $β$ = 84.20 (3), $γ$ = 88.35 (4)°; volume, V = 2830 Å³; molecular formula, Fe₃PO₁₁N₂C₂₃H₁₉; formula weight, 697.9; formula units per cell, Z = 4; density, $ρ$ = 1.64 g cm⁻³; absorption coefficient, $μ$ = 16.3 cm⁻¹; radiation (Mo Kα), λ = 0.71073 Å; collection range, 4° ≤ 2θ ≤ 40°; scan width, Δθ = (0.90 + 0.35 tan θ)°; maximum scan time, 90 s; scan speed range, 0.7–5.0° min⁻¹; total data collected, 5271; independent data, $I > 3σ(I)$, 4192; total variables, 601; $R = \sum||F_o| - |F_c||/\sum|F_o|$, 0.030; $R_w = [\sum w(|F_o| - |F_c|)^2/\sum w|F_o|^2]^{1/2}$, 0.030; weights $w = σ(F)^{-2}$. The Laue symmetry was determined to be 1̄, and the space group was shown to be either P1 or P1̄. Intensities were measured by using the θ–2θ scan technique, with the scan rate depending on the net count obtained in rapid prescans of each reflection. Two standard reflections were monitored periodically during the course of the data collection as a check of crystal stability and electronic reliability, and these did not vary significantly. In reducing the data, Lorentz and polarization factors were applied, as well as an empirical absorption correction based on azimuthal ψ scans of six reflections having χ near 90°.[60] The structure was solved by MULTAN,[61] which revealed the positions of the six Fe and two P atoms

(60) North, A. C. T.; Phillips, D. C.; Matthews, F. S. *Acta Crystallogr., Sect A: Cryst. Phys., Diffr., Theor. Gen. Crystallogr.* **1971**, *A27*, 368.

(61) Germain, G.; Main, P.; Woolfson, M. M. *Acta Crystallogr., Sect. A: Cryst. Phys., Diffr., Theor. Gen. Crystallogr.* **1971**, *A27*, 368.

(62) In this paper the periodic group notation in parentheses is in accord with recent actions by IUPAC and ACS nomenclature committees. A and B notation is eliminated because of wide confusion. Groups IA and IIA become groups 1 and 2. The d-transition elements comprise groups 3 through 12, and the p-block elements comprise groups 13–18. (Note that the former Roman number designation is preserved in the last digit of the new numbering: e.g., III → 3 and 13.)

in the asymmetric unit, which comprises two complete independent molecules. The remaining non-hydrogen atoms were located in subsequent difference Fourier syntheses, after which all hydrogens were entered in ideal calculated positions. All non-hydrogen atoms except the phenyl carbons were refined anisotropically. After all shift/esd ratios were less than 0.1, convergence was reached at the agreement factors listed above. No unusually high correlations were noted between any of the variables in the last cycle of least-squares refinement, and the final difference density map showed no peaks greater than 0.40 e/Å³. All calculations were made with Molecular Structure Corp.'s TEXRAY 230 modifications of the SDP-PLUS series of programs.

The two independent molecules of Fe₃(CO)₈(μ₂-NPh)₂[P(OMe)₃] in the unit cell differ primarily by the orientation of the phenyl groups, the dihedral angles being

	molecule 1	molecule 2
Fe2–N1–C12–C13	−143	−148
Fe2–N1–C12–C17	39	34
Fe2–N2–C18–C19	143	145
Fe2–N2–C18–C23	−39	−37

for both molecules, the phenyl torsions are far from bisecting the Fe1··· Fe2 side (ideally 180° and 0°) in a direction away from the P(OMe)₃ ligand. The latter suggests a steric origin to the conformation. In each
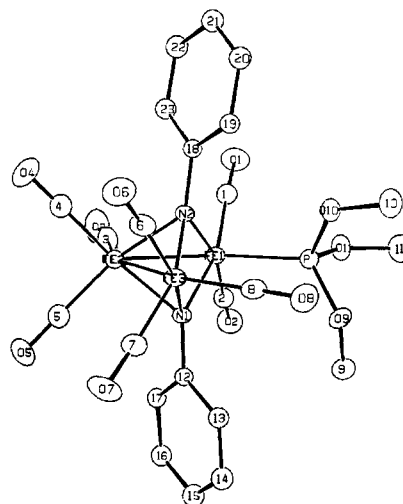
molecule the ortho hydrogen atoms eclipse one CO ligand, which is coplanar with the Fe₃ core at Fe2 (i.e. C3). Thus, it appears that the origin of the phenyl twist is to avoid the other pair of carbonyls on Fe2, with little or no concern about the disposition of P(OMe)₃. In both molecules, the Fe–Fe bond, which is anti to the planar CO on Fe2, is shorter by ~0.06 Å. A similar difference is apparent in the structure of the N-methyl analogue.[28] Thus phosphite substitution has little effect on the structure of the triiron carbonyl cluster. The final atomic parameters and important bond lengths for one of the independent molecules are listed in Tables IX and X, respectively.

Supplementary Material Available: Listing of observed and calculated structure factors for Fe₃(CO)₈(μ₃-PPh)₂[P(OMe)₃] (21 pages). Ordering information is given on any current masthead page.